arXiv:1608.00644v1 [math.NA] 1 Aug 2016

MONOTONE MIXED NARROW/WIDE STENCIL FINITE DIFFERENCE SCHEME FOR MONGE-AMPÈRE EQUATION

YANGANG CHEN* AND JUSTIN W. L. WAN†

Abstract. In this paper, we propose a monotone mixed narrow/wide stencil finite difference scheme for solving the two-dimensional Monge-Ampère equation. In order to accomplish this, we convert the Monge-Ampère equation to an equivalent Hamilton-Jacobi-Bellman (HJB) equation, which is numerically more manageable. Based on the HJB formulation, we apply narrow stencil discretization, which is second order accurate, to the grid points wherever monotonicity holds, and apply wide stencil discretization elsewhere to ensure monotonicity on the entire computational domain. To solve the discretized system, policy iteration is implemented. By dividing the admissible control set into six regions and optimizing the sub-problem in each region, the computational cost of the optimization problem at each grid point in one policy iteration is reduced from $O(M^2)$ to $O(M)$, where the control grid is $M \times M$. We prove that our numerical scheme satisfies consistency, stability and monotonicity, and hence is convergent to the viscosity solution of the Monge-Ampère equation. In the numerical results, second order convergence rate is achieved for smooth solutions and up to order one convergence is achieved for non-smooth solutions.

Key words. nonlinear elliptic partial differential equations, Monge-Ampère equations, Hamilton-Jacobi-Bellman equations, viscosity solutions, finite difference methods, monotone schemes

AMS subject classifications. 35J96, 65N06, 65N12, 65N22

1. Introduction.

The goal of this paper is to compute the numerical solution of the two-dimensional Monge-Ampère equation with Dirichlet boundary condition:

$$\begin{aligned} u_{xx}u_{yy} - u_{xy}^2 &= f, && \text{in } \Omega, \\ u &= g, && \text{on } \partial\Omega, \\ u &\text{ is convex}, \end{aligned} \tag{1.1}$$

where Ω is a bounded convex domain in $\mathbb{R}^2$, $\partial\Omega$ is its boundary, $u : \Omega \to \mathbb{R}$ is the unknown function, and $f : \Omega \to \mathbb{R}$ and $g : \partial\Omega \to \mathbb{R}$ are given functions.

The Monge-Ampère equation is of great interest due to a wide range of applications. One is the prescribed Gaussian curvature problem. More specifically, given the Gaussian curvature of a certain hypersurface, it is possible to find the hypersurface by solving its associated Monge-Ampère equation. Another application is the optimal mass transport (or Monge-Kantorovich) problem. By solving a Monge-Ampère equation, we are able to find the optimal transformation from one density function to another with minimal transportation cost. This further motivates the applications of the Monge-Ampère equation in image registration, mesh generation, etc. We direct the interested readers to [1] for an extensive review of applications.

The Monge-Ampère equation is a fully nonlinear partial differential equation (PDE), since the left hand side consists of products of the second derivatives. As a result, it may have multiple weak solutions. Among all these weak solutions, we are interested in computing the viscosity solution [9, 8], since it is often considered the correct one in many practical applications [14]. In addition, the viscosity solution of the Monge-Ampère equation is globally convex (while the other solutions may not be

*Department of Applied Mathematics, University of Waterloo, 200 University Avenue West, Waterloo, ON, N2L 3G1, Canada.

†Cheriton School of Computer Science, University of Waterloo, 200 University Avenue West, Waterloo, ON, N2L 3G1, Canada.

convex) [14]. Due to the nonlinearity, it is challenging to design a numerical scheme that converges to the viscosity solution.

Some numerical schemes for the Monge-Ampère equation have been proposed in recent years. One approach is using finite difference methods. Some finite difference schemes, such as [4], use standard central differencing to discretize u_{xy}, and are thus not monotone. The significance of monotonicity is that together with consistency and stability, they provide sufficient conditions for a numerical scheme to converge to the viscosity solution [3]. To the best of our knowledge, there exist two numerical schemes that are monotone and thus convergent in the viscosity sense. One scheme is to exploit the geometrical interpretation of the Monge-Ampère equation [22]. The grid structure, constrained by the geometry of the equation, is usually not rectangular or triangular. The other scheme, proposed in [21, 14], achieves monotonicity using a large number of stencil points. In order for the scheme to converge, the number of the stencil points must increase towards infinity when the mesh size h decreases towards 0, thus resulting in high computational costs for solving problems on fine grids.

Another approach for the Monge-Ampère equation is using Galerkin-type methods. An immediate challenge is that it is not obvious how to write down the variational formulation of (1.1) using the common integration-by-parts approach. The L^2 projection methods, proposed in [5, 7], build up the Galerkin-type schemes based on the linearized Monge-Ampère equation, and is convergent for $H^2(\Omega)$. In [10], the authors reformulate the Monge-Ampère equation into an augmented Lagrangian problem or a least-squares problem, which allows the use of mixed finite element methods. It is unclear whether these Galerkin-type schemes converge for the non-regular solutions. The authors in [12] add an artificial fourth order elliptic differential operator $\epsilon\Delta^2 u$. They show that with this additional term, a variational formulation, and thus a finite element scheme, becomes possible. That being said, in the error analysis, the error can grow to infinity as $\epsilon \to 0$.

Instead of solving the Monge-Ampère equation (1.1) directly, as many of the existing methods do, our approach is to first convert (1.1) into an equivalent Hamilton-Jacobi-Bellman (HJB) equation [17, 19]. As will become clear, the idea of using HJB formulation is that solving the equivalent HJB equation is numerically more tractable than solving (1.1) directly, since the differential operator of the HJB equation under fixed control parameters is linear. To the best of our knowledge, our work is the first application of the HJB formulation in the numerical computation of the Monge-Ampère equation.

Our next goal is to design a monotone finite difference scheme for the equivalent HJB equation. We note that the cross derivative u_{xy} is still present in the HJB equation, and the standard central differencing for u_{xy} may be non-monotone. Our approach is to apply a mixed narrow/wide stencil discretization at each grid point. More specifically, narrow stencil discretization (or standard 7-point stencil discretization) is used to discretize u_{xy} at a grid point, if the narrow stencil discretization is monotone. Otherwise, a local coordinate rotation is performed to remove the cross derivative from the HJB equation, and then a wide stencil discretization is implemented [11, 20]. We emphasize that our discretization scheme is designed such that consistency, stability and monotonicity are fulfilled. As a result, our numerical scheme is guaranteed to converge to the viscosity solution of the Monge-Ampère equation [3]. Meanwhile, by maximal use of narrow stencil discretization, which is second order accurate, our numerical scheme can achieve small error and fast convergence.

To solve the resulting nonlinear discretized system, a Newton-like fixed point

iteration, called policy iteration, can be implemented [16, 13]. One major concern of implementing policy iteration is that each iteration requires solving an optimization problem over an admissible control set at each grid point. Typically bilinear search is used, and its complexity is $O(M^2)$, where the control grid is $M \times M$. Our approach is to divide the admissible control set into six regions and find an effective method to solve the optimization problem in each region. Consequentially, the computational cost is reduced from $O(M^2)$ to $O(M)$.

To illustrate our numerical scheme, in Section 2, we will establish the equivalent HJB formulation for the Monge-Ampère equation (1.1). In Section 3, we will describe our mixed narrow/wide stencil finite difference discretization for the HJB formulation. Section 4 solves the nonlinear discretized system using policy iteration. Section 5 proves that our numerical scheme is consistent, stable and monotone, and thus converges to the viscosity solution of (1.1). Section 6 shows numerical results where some solutions are smooth and some are not. We also demonstrate the rate of convergence for each case.

2. HJB Formulation of Monge-Ampère Equation. The objective of this paper is to compute the viscosity solution of the Monge-Ampère equation (1.1). An overview on the topic of viscosity solution can be found in [9, 8]. Before defining the viscosity solution of (1.1), we rewrite (1.1) as

$$\mathcal{F}\left(\mathbf{x}, D^2u(\mathbf{x})\right) \equiv -\det\left[D^2u(\mathbf{x})\right] + f(\mathbf{x}) = 0, \tag{2.1}$$

where $\mathbf{x} = (x, y) \in \Omega$, and D^2u is the Hessian matrix of u.

DEFINITION 2.1 (Viscosity solution of the Monge-Ampère equation).

The convex function $u \in C(\Omega)$ is a viscosity sub-solution (or super-solution) of the Monge-Ampère equation $\mathcal{F}\left(\mathbf{x}, D^2u(\mathbf{x})\right) = 0$, if for all the test functions $\varphi(\mathbf{x}) \in C^2(\Omega)$ and all $\mathbf{x} \in \Omega$, such that $u - \varphi$ has a local maximum (or minimum) at $\mathbf{x}$, we have

$$\mathcal{F}_*(\mathbf{x}, D^2\varphi(\mathbf{x})) \le 0 \quad \left(\text{ or } \mathcal{F}^*(\mathbf{x}, D^2\varphi(\mathbf{x})) \ge 0 \right), \tag{2.2}$$

where $\mathcal{F}_*$ (or $\mathcal{F}^*$) is the lower (or upper) semi-continuous envelope of $\mathcal{F} : C \to \mathbb{R}$ on a closed set C, defined as:

$$\mathcal{F}_*(x) = \liminf_{\substack{y \to x \\ y \in C}} \mathcal{F}(y) \qquad \left(\text{ or } \mathcal{F}^*(x) = \limsup_{\substack{y \to x \\ y \in C}} \mathcal{F}(y) \right). \tag{2.3}$$

Furthermore, the function u is a viscosity solution if it is both a viscosity sub-solution and super-solution.

We note that u is a convex function, or equivalently, D^2u is positive semi-definite, which implies that $\det(D^2u) = f \ge 0$. This condition indicates that the differential operator of (2.1) is degenerate elliptic. Furthermore, degenerate ellipticity, plus Ω being bounded and convex, ensures the existence and uniqueness of the viscosity solution of (1.1), and that the comparison principle holds. See[8, 15] for details.

Since the Monge-Ampère equation (1.1) is nonlinear, it is challenging to design a finite difference scheme that converges to the viscosity solution. Our approach is to convert the Monge-Ampère equation into an equivalent HJB equation. The equivalence of the two PDEs is first established in [17] and [19] for arbitrary dimensions. We include the two-dimensional version as follows:

LEMMA 2.2. *Let $B \in \mathbb{R}^{2\times 2}$ be a symmetric matrix and let $c \ge 0$. Define the set*

$$S_1^+ \equiv \{A \in \mathbb{R}^{2\times 2} : A \text{ is positive semi-definite}, A^T = A, \operatorname{tr}(A) = 1\}. \tag{2.4}$$

Then B satisfies

$$\max_{A\in S_1^+}\left\{\operatorname{tr}(AB)+c\sqrt{\det(A)}\right\}=0, \tag{2.5}$$

if and only if

$$\begin{aligned} &B \text{ is negative semi-definite},\\ &2\sqrt{\det(-B)}=c. \end{aligned} \tag{2.6}$$

Proof. See Appendix A. ∎

This lemma can be applied to reformulate the Monge-Ampère equation into an HJB equation:

THEOREM 2.3. *Let Ω be a convex open set in $\mathbb{R}^2$. Let $u\in C^2(\Omega)$ be convex, and $f\in C(\Omega)$ be a non-negative function. Then u solves the Monge-Ampère equation (1.1) if and only if it solves the following HJB equation,*

$$\max_{A(\mathbf{x})\in S_1^+}\left\{-\operatorname{tr}\left[A(\mathbf{x})D^2u(\mathbf{x})\right]+2\sqrt{\det(A(\mathbf{x}))\,f(\mathbf{x})}\right\}=0, \tag{2.7}$$

where S_1^+ is defined in (2.4) and $A(\mathbf{x})\in S_1^+$ is the control at point $\mathbf{x}$.

Proof. Apply Lemma 2.2. Let $c=2\sqrt{f}$ and $B=-D^2u$. Equation (2.5) becomes (2.7), and Equation (2.6) becomes (2.1), or equivalently, (1.1). ∎

We notice that due to the positive semi-definite property of the matrix $A(\mathbf{x})$, it can be diagonalized by a two-dimensional orthogonal matrix. More specifically, $A(\mathbf{x})\in S_1^+$ can be parametrized as follows:

$$\begin{aligned} A(\mathbf{x})=&\begin{pmatrix}\cos\theta(\mathbf{x}) & \sin\theta(\mathbf{x})\\ -\sin\theta(\mathbf{x}) & \cos\theta(\mathbf{x})\end{pmatrix}\begin{pmatrix}a(\mathbf{x}) & 0\\ 0 & 1-a(\mathbf{x})\end{pmatrix}\begin{pmatrix}\cos\theta(\mathbf{x}) & -\sin\theta(\mathbf{x})\\ \sin\theta(\mathbf{x}) & \cos\theta(\mathbf{x})\end{pmatrix},\\ &a(\mathbf{x})\in[0,1],\theta(\mathbf{x})\in[-\pi,\pi). \end{aligned} \tag{2.8}$$

This parametrization gives rise to the following HJB equation, which we aim at solving.

COROLLARY 2.4. *Under the parametrization (2.8), the HJB equation (2.7) becomes*

$$\begin{aligned} \max_{(a(\mathbf{x}),\theta(\mathbf{x}))\in\Gamma}\quad &\{-\alpha_{11}(a(\mathbf{x}),\theta(\mathbf{x}))u_{xx}(\mathbf{x})-2\alpha_{12}(a(\mathbf{x}),\theta(\mathbf{x}))u_{xy}(\mathbf{x})\\ &-\alpha_{22}(a(\mathbf{x}),\theta(\mathbf{x}))u_{yy}(\mathbf{x})+2\sqrt{a(\mathbf{x})(1-a(\mathbf{x}))f(\mathbf{x})}\Big\}=0, \end{aligned} \tag{2.9}$$

where $(a(\mathbf{x}),\theta(\mathbf{x}))$ is the pair of controls at point $\mathbf{x}$, $\Gamma=[0,1]\times\left[-\frac{\pi}{4},\frac{\pi}{4}\right)$ is the set of admissible controls[1] *, and the coefficients are*

$$\begin{aligned} \alpha_{11}(a(\mathbf{x}),\theta(\mathbf{x})) &= \frac{1}{2}[1-(1-2a(\mathbf{x}))\cos 2\theta(\mathbf{x})],\\ \alpha_{22}(a(\mathbf{x}),\theta(\mathbf{x})) &= \frac{1}{2}[1+(1-2a(\mathbf{x}))\cos 2\theta(\mathbf{x})],\\ \alpha_{12}(a(\mathbf{x}),\theta(\mathbf{x})) &= \frac{1}{2}(1-2a(\mathbf{x}))\sin 2\theta(\mathbf{x}). \end{aligned} \tag{2.10}$$

[1] Although (2.8) defines the admissible control set to be in the range of $[0,1]\times[-\pi,\pi)$, the optimal control pair (a^*,θ^*) that maximizes (2.9) may not be unique in $[0,1]\times[-\pi,\pi)$. We notice that since $\mathcal{L}_{a,\theta}u=\mathcal{L}_{a,\theta+\pi}u$, and $\mathcal{L}_{a,\theta}u=\mathcal{L}_{1-a,\theta+\frac{\pi}{2}}u$, the admissible control set Γ can be reduced to $[0,1]\times[-\frac{\pi}{4},\frac{\pi}{4})$. Such removal of the redundancy of Γ ensures that the optimal control pair (a^*,θ^*) is unique in Γ, except when $a^*=\frac{1}{2}$ or when $f=0$.

For convenience, we rewrite the HJB equation (2.9) as

$$\mathcal{F}\left(\mathbf{x}, D^2u(\mathbf{x})\right) \equiv \max_{(a(\mathbf{x}),\theta(\mathbf{x}))\in\Gamma} \mathcal{L}_{a(\mathbf{x}),\theta(\mathbf{x})}\, u(\mathbf{x}) = 0, \tag{2.11}$$

where the differential operator of the HJB equation is given by

$$\mathcal{L}_{a,\theta}\, u \equiv -\alpha_{11}(a,\theta)u_{xx} - 2\alpha_{12}(a,\theta)u_{xy} - \alpha_{22}(a,\theta)u_{yy} + 2\sqrt{a(1-a)f}. \tag{2.12}$$

We note that since the HJB equation (2.11)-(2.12) and the Monge-Ampère equation (2.1) are mathematically equivalent, we still use the notation $\mathcal{F}\left(\mathbf{x}, D^2u(\mathbf{x})\right)$ to denote the HJB equation.

A useful property of the HJB equation is that for a fixed given control pair (a,θ), the differential operator $\mathcal{L}_{a,\theta}\, u$ is linear. We note, however, that the HJB equation itself is still nonlinear, since the maximization depends on u. Unlike (1.1), the linear differential operator $\mathcal{L}_{a,\theta}\, u$ does not contain products of the second derivatives. Hence, the HJB equation is more manageable than (1.1). More importantly, the linearity of $\mathcal{L}_{a,\theta}\, u$ allows us to develop finite difference schemes based on numerical methods for linear PDEs. Our approach is then to solve the HJB equation (2.9) instead of the Monge-Ampère equation (1.1).

3. Mixed Narrow/Wide Stencil Finite Difference Discretization. In this section, we will construct a monotone finite difference discretization for the HJB equation (2.9). We note that monotonicity is a desirable property, since [3] has proved that monotonicity is one of the sufficient conditions for a numerical scheme to converge to the viscosity solution.

To set up notation, let us consider an $N \times N$ square grid $\{\mathbf{x}_{i,j} = (x_i, y_j)\}$, where $\mathbf{x}_{i,j} \in \Omega$ when $i,j = 1,\cdots,N$, and $\mathbf{x}_{i,j} \in \partial\Omega$ when $i,j = 0$ or $N+1$. Also, let h be the mesh size and let $U_{i,j}$ be the discrete approximation of $u(\mathbf{x}_{i,j})$. We aim at solving the set of the unknowns $\{U_{i,j} \,|\, 1 \le i \le N, 1 \le j \le N\}$.

3.1. Narrow stencil discretization. Consider discretizing the HJB equation (2.9) at a grid point $\mathbf{x}_{i,j}$. We can use standard central differencing for $u_{xx}(\mathbf{x}_{i,j})$ and $u_{yy}(\mathbf{x}_{i,j})$:

$$\begin{aligned} u_{xx}(\mathbf{x}_{i,j}) &\approx (U_{xx})_{i,j} \equiv \frac{1}{h^2}(U_{i+1,j} - 2U_{i,j} + U_{i-1,j}), \\ u_{yy}(\mathbf{x}_{i,j}) &\approx (U_{yy})_{i,j} \equiv \frac{1}{h^2}(U_{i,j+1} - 2U_{i,j} + U_{i,j-1}). \end{aligned} \tag{3.1}$$

It can be shown that standard 7-point stencil discretization for $u_{xy}(\mathbf{x}_{i,j})$ can lead to a monotone scheme in the following two cases:

- When

$$\alpha_{11}(a_{i,j},\theta_{i,j}) \ge |\alpha_{12}(a_{i,j},\theta_{i,j})|,\ \alpha_{22}(a_{i,j},\theta_{i,j}) \ge |\alpha_{12}(a_{i,j},\theta_{i,j})|, \quad \text{and } \alpha_{12}(a_{i,j},\theta_{i,j}) \ge 0, \tag{3.2}$$

where $(a_{i,j},\theta_{i,j}) \equiv (a(\mathbf{x}_{i,j}),\theta(\mathbf{x}_{i,j}))$, we use

$$\begin{aligned} u_{xy}(\mathbf{x}_{i,j}) \approx (U_{xy})^{(1)}_{i,j} \equiv\ & \frac{1}{2h^2}(2U_{i,j} + U_{i+1,j+1} + U_{i-1,j-1} \\ & -U_{i+1,j} - U_{i-1,j} - U_{i,j+1} - U_{i,j-1}). \end{aligned} \tag{3.3}$$

- When

$$\alpha_{11}(a_{i,j},\theta_{i,j}) \geq |\alpha_{12}(a_{i,j},\theta_{i,j})|,\ \alpha_{22}(a_{i,j},\theta_{i,j}) \geq |\alpha_{12}(a_{i,j},\theta_{i,j})|, \quad \text{and } \alpha_{12}(a_{i,j},\theta_{i,j}) \leq 0, \tag{3.4}$$

we use

$$u_{xy}(\mathbf{x}_{i,j}) \approx (U_{xy})^{(2)}_{i,j} \equiv \frac{1}{2h^2}(-2U_{i,j} - U_{i+1,j-1} - U_{i-1,j+1} + U_{i+1,j} + U_{i-1,j} + U_{i,j+1} + U_{i,j-1}). \tag{3.5}$$

We remark that Condition (3.2) and Condition (3.4) depend on the coefficients α_{11}, α_{22} and α_{12}, which in turn depend on the pair of controls $(a_{i,j},\theta_{i,j})$.

If either (3.2) or (3.4) is satisfied at $\mathbf{x}_{i,j}$, then the finite difference discretization of (2.9) is given by

$$\max_{(a_{i,j},\theta_{i,j})\in\Gamma} \Big\{ -\alpha_{11}(a_{i,j},\theta_{i,j})(U_{xx})_{i,j} - 2\alpha_{12}(a_{i,j},\theta_{i,j})(U_{xy})^{(disc)}_{i,j} - \alpha_{22}(a_{i,j},\theta_{i,j})(U_{yy})_{i,j} + 2\sqrt{a_{i,j}(1-a_{i,j})f_{i,j}} \Big\} = 0, \tag{3.6}$$

where $f_{i,j} = f(\mathbf{x}_{i,j})$, and

$$disc = \begin{cases} 1, & \text{if Condition (3.2) is satisfied,} \\ 2, & \text{if Condition (3.4) is satisfied.} \end{cases} \tag{3.7}$$

3.2. Wide stencil discretization. However, if neither (3.2) nor (3.4) is fulfilled at the grid point $\mathbf{x}_{i,j}$, then it is unclear how to directly discretize the cross derivative $u_{xy}(\mathbf{x}_{i,j})$ in (2.9) monotonically. Our approach, following [11] and [20], is to eliminate the cross derivative $u_{xy}(\mathbf{x}_{i,j})$ by a local coordinate transformation. Let $\{(\mathbf{e}_z)_{i,j},(\mathbf{e}_w)_{i,j}\}$ be a local orthogonal basis which is obtained by a rotation of the standard axes $\{(\mathbf{e}_x)_{i,j},(\mathbf{e}_y)_{i,j}\}$ at an angle $\phi_{i,j}$; see Figure 3.1. More precisely,

$$\begin{pmatrix}(\mathbf{e}_z)_{i,j} & (\mathbf{e}_w)_{i,j}\end{pmatrix} = \begin{pmatrix}\cos\phi_{i,j} & -\sin\phi_{i,j} \\ \sin\phi_{i,j} & \cos\phi_{i,j}\end{pmatrix} \begin{pmatrix}(\mathbf{e}_x)_{i,j} & (\mathbf{e}_y)_{i,j}\end{pmatrix}. \tag{3.8}$$

If the rotation angle $\phi_{i,j}$ is chosen to be

$$\phi_{i,j} = \frac{1}{2}\arctan\frac{2\alpha_{12}\left(a_{i,j},\theta_{i,j}\right)}{\alpha_{11}\left(a_{i,j},\theta_{i,j}\right) - \alpha_{22}\left(a_{i,j},\theta_{i,j}\right)} = -\theta_{i,j}, \tag{3.9}$$

then the cross derivative vanishes under the basis $\{(\mathbf{e}_z)_{i,j},(\mathbf{e}_w)_{i,j}\}$. By straightforward algebra, one can show that (2.9) becomes

$$\max_{(a_{i,j},\theta_{i,j})\in\Gamma} \left\{ -a_{i,j}\, u_{zz}(\mathbf{x}_{i,j}) - (1-a_{i,j})\ u_{ww}(\mathbf{x}_{i,j}) + 2\sqrt{a_{i,j}\left(1-a_{i,j}\right) f_{i,j}} \right\} = 0. \tag{3.10}$$

Here $u_{zz}(\mathbf{x}_{i,j})$ and $u_{ww}(\mathbf{x}_{i,j})$ are the directional derivatives along the basis $(\mathbf{e}_z)_{i,j}$ and $(\mathbf{e}_w)_{i,j}$ respectively. We remark that their coefficients $-a_{i,j}$ and $-(1-a_{i,j})$ are independent from the control $\theta_{i,j}$, while the directions of $(\mathbf{e}_z)_{i,j}$ and $(\mathbf{e}_w)_{i,j}$ depend on $\theta_{i,j}$. Since $a_{i,j} \in [0,1]$, the two coefficients are always non-positive, which is equivalent to the fact that (3.10) is an elliptic PDE.

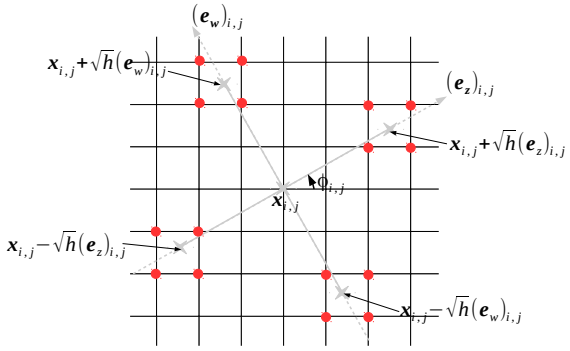

FIG. 3.1. *Local coordinate rotation at the grid point $\mathbf{x}_{i,j}$, and wide stencil discretization of $u_{zz}(\mathbf{x}_{i,j})$ and $u_{ww}(\mathbf{x}_{i,j})$ under the rotation. The rotation angle is $\phi_{i,j}$, counter-clockwise. The grey dashed lines are the orthogonal axis $\{(\mathbf{e}_z)_{i,j}, (\mathbf{e}_w)_{i,j}\}$. The grey stars are the stencil points. Since the stencil points may not coincide with any grid points, in order to approximate u at these stencil points, bilinear interpolation from the neighbouring points (red dots) is needed. In order to maintain consistency, stencil length $\sqrt{h}$ is chosen. Note that $\sqrt{h} > h$. As a result, the four wide stencil points (grey stars) are $\mathbf{x}_{i,j} \pm \sqrt{h}(\mathbf{e}_z)_{i,j}$ and $\mathbf{x}_{i,j} \pm \sqrt{h}(\mathbf{e}_w)_{i,j}$, and standard central differencing associated with this wide stencil is applied to approximate $u_{zz}(\mathbf{x}_{i,j})$ and $u_{ww}(\mathbf{x}_{i,j})$.*

To complete the finite difference discretization in (3.10), we apply standard central differencing to $u_{zz}(\mathbf{x}_{i,j})$ and $u_{ww}(\mathbf{x}_{i,j})$. For instance, we approximate $u_{zz}(\mathbf{x}_{i,j})$ by $\frac{1}{h^2}\left[u(\mathbf{x}_{i,j} + h(\mathbf{e}_z)_{i,j}) - 2U_{i,j} + u(\mathbf{x}_{i,j} - h(\mathbf{e}_z)_{i,j})\right]$. However, since the stencil is rotated, the stencil points $\mathbf{x}_{i,j} \pm h(\mathbf{e}_z)_{i,j}$ may no longer coincide with any grid points. In such cases, bilinear interpolation from the neighbouring grid points can be used to approximate $u(\mathbf{x}_{i,j} \pm h(\mathbf{e}_z)_{i,j})$. However, a consequence of the bilinear interpolation is that the truncation error of this central difference approximation becomes $O(1)$ if the stencil length is h. In order to maintain consistency, we choose the stencil length $\sqrt{h}$, which yields $O(h)$ truncation error. Note that when h is small, $\sqrt{h} > h$, which means the stencil length appears to be wide. Figure 3.1 explains the details of this wide stencil discretization. As a result, the finite difference discretization for $u_{zz}(\mathbf{x}_{i,j})$ and $u_{ww}(\mathbf{x}_{i,j})$ is given by

(3.11)

$$u_{zz}(\mathbf{x}_{i,j}) \approx (U_{zz})_{i,j} \equiv \frac{1}{h}\left[\mathcal{I}_h U|_{\mathbf{x}_{i,j}+\sqrt{h}(\mathbf{e}_z)_{i,j}} - 2U_{i,j} + \mathcal{I}_h U|_{\mathbf{x}_{i,j}-\sqrt{h}(\mathbf{e}_z)_{i,j}}\right],$$
$$u_{ww}(\mathbf{x}_{i,j}) \approx (U_{ww})_{i,j} \equiv \frac{1}{h}\left[\mathcal{I}_h U|_{\mathbf{x}_{i,j}+\sqrt{h}(\mathbf{e}_w)_{i,j}} - 2U_{i,j} + \mathcal{I}_h U|_{\mathbf{x}_{i,j}-\sqrt{h}(\mathbf{e}_w)_{i,j}}\right],$$

where we have used the stencil length $\sqrt{h}$, and used bilinear interpolation to approximate the unknown values at the stencil points $\mathbf{x}_{i,j} \pm \sqrt{h}(\mathbf{e}_z)_{i,j}$ and $\mathbf{x}_{i,j} \pm \sqrt{h}(\mathbf{e}_w)_{i,j}$, denoted as $\mathcal{I}_h U|_{\mathbf{x}_{i,j}\pm\sqrt{h}(\mathbf{e}_z)_{i,j}}$ and $\mathcal{I}_h U|_{\mathbf{x}_{i,j}\pm\sqrt{h}(\mathbf{e}_w)_{i,j}}$.

If we want to apply the wide stencil discretization at a grid point $\mathbf{x}_{i,j}$ that is close to the boundary, some of its associated stencil points may fall outside the computational domain Ω. In such case, our solution is to shrink the corresponding stencil length(s) such that the resulting stencil point(s) fall onto the boundary $\partial\Omega$. To illustrate the idea, without loss of generality, we focus on the discretization of $u_{zz}(\mathbf{x}_{i,j})$ and consider two scenarios:

Scenario 1. Consider Figure 3.2 (left). Let us assume that $\mathbf{x}_{i,j} + \sqrt{h}(\mathbf{e}_z)_{i,j}$ falls outside Ω. We truncate the corresponding stencil length from $\sqrt{h}$ to η_1 along the

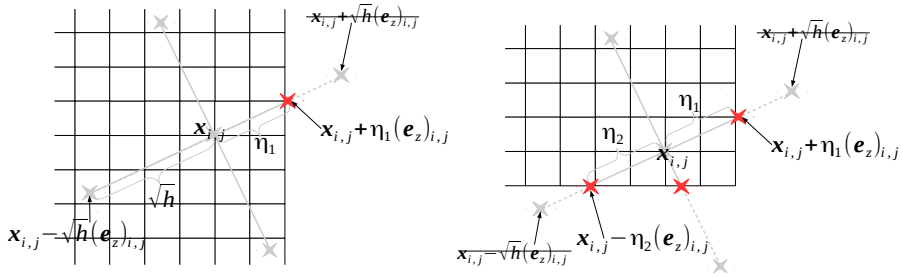

FIG. 3.2. *(left) Scenario 1: One of the wide stencil points* $\mathbf{x}_{i,j} + \sqrt{h}(\mathbf{e}_z)_{i,j}$ *falls outside* Ω. *The wide stencil is truncated and the stencil point is relocated to the point* $\mathbf{x}_{i,j} + \eta_1(\mathbf{e}_z)_{i,j} \in \partial\Omega$ *(labelled by the red star). The corresponding stencil length has shrunk from* $\sqrt{h}$ *to* η_1. *(right) Scenario 2: Both of the wide stencil points* $\mathbf{x}_{i,j} \pm \sqrt{h}(\mathbf{e}_z)_{i,j}$ *fall outside* Ω *and are relocated to the points* $\mathbf{x}_{i,j} + \eta_1(\mathbf{e}_z)_{i,j} \in \partial\Omega$ *and* $\mathbf{x}_{i,j} - \eta_2(\mathbf{e}_z)_{i,j} \in \partial\Omega$ *respectively (labelled by the red stars). The corresponding stencil lengths have shrunk to* η_1 *and* η_2.

$\mathbf{e}_z$ axis, such that the stencil point is relocated to $\mathbf{x}_{i,j} + \eta_1(\mathbf{e}_z)_{i,j} \in \partial\Omega$. Since the two-sided stencil lengths η_1 and $\sqrt{h}$ are not equal, the finite difference approximation for $u_{zz}(\mathbf{x}_{i,j})$ in (3.11) is replaced by

$$u_{zz}(\mathbf{x}_{i,j}) \approx (U_{zz})_{i,j} \equiv \frac{\frac{g(\mathbf{x}_{i,j}+\eta_1(\mathbf{e}_z)_{i,j})-U_{i,j}}{\eta_1} - \frac{U_{i,j}-\mathcal{I}_h U|_{\mathbf{x}_{i,j}-\sqrt{h}(\mathbf{e}_z)_{i,j}}}{\sqrt{h}}}{\frac{\eta_1+\sqrt{h}}{2}}. \tag{3.12}$$

where we have used the Dirichlet boundary condition of (1.1): $u(\mathbf{x}_{i,j} + \eta_1(\mathbf{e}_z)_{i,j}) = g(\mathbf{x}_{i,j} + \eta_1(\mathbf{e}_z)_{i,j})$.

Scenario 2. Consider Figure 3.2 (right). Let us assume that both stencil points $\mathbf{x}_{i,j} \pm \sqrt{h}(\mathbf{e}_z)_{i,j}$ fall outside Ω. We truncate the corresponding stencil lengths to η_1 and η_2. In such case, the finite difference approximation for $u_{zz}(\mathbf{x}_{i,j})$ in (3.11) is changed to

$$u_{zz}(\mathbf{x}_{i,j}) \approx (U_{zz})_{i,j} \equiv \frac{\frac{g(\mathbf{x}_{i,j}+\eta_1(\mathbf{e}_z)_{i,j})-U_{i,j}}{\eta_1} - \frac{U_{i,j}-g(\mathbf{x}_{i,j}-\eta_2(\mathbf{e}_z)_{i,j})}{\eta_2}}{\frac{\eta_1+\eta_2}{2}}. \tag{3.13}$$

We note that such procedure can be used whenever $\mathbf{x}_{i,j}$ is close to the boundary and a truncation of stencil is needed.

To summarize, when neither (3.2) nor (3.4) is satisfied at $\mathbf{x}_{i,j}$, we apply the following wide stencil finite difference discretization to the HJB equation (2.9):

$$\max_{(a_{i,j},\theta_{i,j})\in\Gamma} \left\{ -a_{i,j}\,(U_{zz})_{i,j} - (1-a_{i,j})\,(U_{ww})_{i,j} + 2\sqrt{a_{i,j}\,(1-a_{i,j})\,f_{i,j}} \right\} = 0, \tag{3.14}$$

where $(U_{zz})_{i,j}$ and $(U_{ww})_{i,j}$ are defined by (3.11) when $\mathbf{x}_{i,j}$ is inside the computational domain, and by (3.12), (3.13) or similar expressions when $\mathbf{x}_{i,j}$ is near the boundary.

3.3. The discrete system and its general form. Section 3.1 and 3.2 describe the mixed narrow/wide finite difference discretization. This gives rise to a nonlinear discrete system which contains N^2 discrete equations. To summarize, the discrete equation at each grid point $\mathbf{x}_{i,j}$ is given by the following:

- When the control pair $(a_{i,j}, \theta_{i,j})$ satisfies Condition (3.2) or (3.4), the discrete equation is given by the narrow stencil discretization (3.6).

- Otherwise, the discrete equation is given by the wide stencil discretization (3.14).

One can show that both the narrow stencil discretization (3.6) and the wide stencil discretization (3.14) at the grid point $\mathbf{x}_{i,j}$ can be written into the following general form:

$$\begin{aligned}&\mathcal{F}^h\left(\mathbf{x}_{i,j}, U_{i,j}, \{U_{p,q}|_{(p,q)\neq(i,j)}\}\right)\\ &\equiv \max_{(a_{i,j},\theta_{i,j})\in\Gamma} \mathcal{L}^h\left(\mathbf{x}_{i,j}; a_{i,j}, \theta_{i,j}; U_{i,j}, \{U_{p,q}|_{(p,q)\neq(i,j)}\}\right) = 0,\end{aligned} \tag{3.15}$$

where

$$\begin{aligned}&\mathcal{L}^h\left(\mathbf{x}_{i,j}; a_{i,j}, \theta_{i,j}; U_{i,j}, \{U_{p,q}|_{(p,q)\neq(i,j)}\}\right)\\ &\equiv A_{i,j}(a_{i,j},\theta_{i,j})\,U_{i,j} - \sum_{(p,q)\neq(i,j)} A_{p,q}(a_{i,j},\theta_{i,j})\,U_{p,q} - F_{i,j}(a_{i,j},\theta_{i,j}).\end{aligned} \tag{3.16}$$

Here the symbols $\mathcal{F}^h$ and $\mathcal{L}^h$ in (3.15)-(3.16) represent the discretization of $\mathcal{F}$ and $\mathcal{L}$ in (2.11)-(2.12). $A_{i,j}(a_{i,j},\theta_{i,j})$ and $A_{p,q}(a_{i,j},\theta_{i,j})$ are the coefficients of the unknowns $U_{i,j}$ and $U_{p,q}$, respectively, and $F_{i,j}(a_{i,j},\theta_{i,j})$ is the collection of the terms that do not explicitly contain unknown U.

We note that $A_{i,j}(a_{i,j},\theta_{i,j})$, $A_{p,q}(a_{i,j},\theta_{i,j})$ and $F_{i,j}(a_{i,j},\theta_{i,j})$ depend on $(a_{i,j},\theta_{i,j})$ and satisfy the following properties:

$$A_{i,j}(a_{i,j},\theta_{i,j}) > 0, \quad -A_{p,q}(a_{i,j},\theta_{i,j}) \le 0, \tag{3.17}$$

$$A_{i,j}(a_{i,j},\theta_{i,j}) - \sum_{(p,q)\neq(i,j)} A_{p,q}(a_{i,j},\theta_{i,j}) \ge 0. \tag{3.18}$$

These properties are crucial for the numerical scheme to be stable and monotone, as will be shown in Section 5.

To show how the narrow stencil discretization (3.6) and the wide stencil discretization (3.14) can be written into the general form (3.15)-(3.16), we analyze three cases.

Case 1. This is illustrated in Figure 3.3 (left-top). Suppose Condition (3.2) is satisfied at $\mathbf{x}_{i,j}$. Then we use the narrow stencil discretization (3.6) with $disc = 1$. Some simple algebra can transform (3.6) into the following:

$$\begin{aligned}\max_{(a_{i,j},\theta_{i,j})\in\Gamma} \Big\{ &\frac{2}{h^2}(\alpha_{11}+\alpha_{22}-\alpha_{12})U_{i,j} - \frac{1}{h^2}(\alpha_{11}-\alpha_{12})U_{i+1,j} - \frac{1}{h^2}(\alpha_{11}-\alpha_{12})U_{i-1,j}\\ &-\frac{1}{h^2}(\alpha_{22}-\alpha_{12})U_{i,j+1} - \frac{1}{h^2}(\alpha_{22}-\alpha_{12})U_{i,j-1} - \frac{1}{h^2}\alpha_{12}U_{i+1,j+1} - \frac{1}{h^2}\alpha_{12}U_{i-1,j-1}\\ &+2\sqrt{a_{i,j}(1-a_{i,j})f_{i,j}}\Big\} = 0,\end{aligned} \tag{3.19}$$

where we have suppressed the dependency of the coefficients on $(a_{i,j},\theta_{i,j})$. This equation has the form of (3.15)-(3.16), and contains 7 unknown values of U. Under Condition (3.2), it is easy to verify that (3.17) and (3.18) are true. We also note that equal sign is achieved in (3.18).

Case 2. This is illustrated in Figure 3.3 (left-bottom). Consider the same setting as Case 1, except that the grid point $\mathbf{x}_{i,j}$ is near the boundary. Without loss of generality, let us assume that $\mathbf{x}_{i,j} = \mathbf{x}_{1,N}$. Now that $U_{0,N}$, $U_{1,N+1}$, $U_{2,N+1}$ and

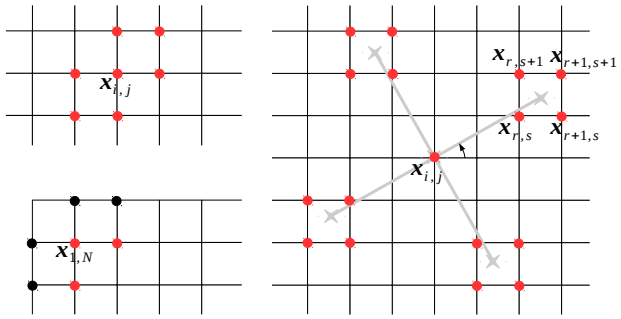

FIG. 3.3. *(left-top) Case 1: Suppose Condition (3.2) is satisfied at* $\mathbf{x}_{i,j}$ *and narrow stencil discretization (3.6) is used. The discrete equation contains 7 unknown values of* U*, labelled by the red dots. (left-bottom) Case 2: Consider* $\mathbf{x}_{1,N}$*, which is close to the boundary. The black dots sit on the boundary and the values of* U *on these points are determined by the Dirichlet boundary condition. As a result, the discrete equation contains 3 unknown values of* U*, labelled by the red dots. (right) Case 3: Suppose neither (3.2) nor (3.4) is satisfied at* $\mathbf{x}_{i,j}$ *and thus wide stencil discretization (3.14) is used. Since bilinear interpolation of each stencil point contains 4 unknown values, the resulting discrete equation has 17 unknown values in total.*

$U_{0,N-1}$ can be determined by the Dirichlet boundary condition $u = g$ in (1.1), (3.19) is changed to

(3.20)
$$\max_{(a_{1,N},\theta_{1,N})\in\Gamma}\left\{\frac{2}{h^2}(\alpha_{11}+\alpha_{22}-\alpha_{12})U_{1,N}-\frac{1}{h^2}(\alpha_{11}-\alpha_{12})U_{2,N}-\frac{1}{h^2}(\alpha_{22}-\alpha_{12})U_{1,N-1}\right.$$
$$+2\sqrt{a_{1,N}(1-a_{1,N})f_{1,N}}-\frac{1}{h^2}\alpha_{12}g_{2,N+1}-\frac{1}{h^2}\alpha_{12}g_{0,N-1}$$
$$\left.-\frac{1}{h^2}(\alpha_{11}-\alpha_{12})g_{0,N}-\frac{1}{h^2}(\alpha_{22}-\alpha_{12})g_{1,N+1}\right\}=0.$$

Case 2 is essentially the same as Case 1, except that (3.20) contains only 3 unknown values, $F_{i,j}(a_{i,j},\theta_{i,j})$ contains the contribution from the boundary condition, and (3.18) is valid in the strict inequality sense.

Case 3. See Figure 3.3 (right) for the illustration. Suppose neither (3.2) nor (3.4) is fulfilled at $\mathbf{x}_{i,j}$, so wide stencil discretization (3.14) is implemented. We also assume that $\mathbf{x}_{i,j}$ is inside the computational domain and no stencil truncation occurs. Then (3.14) can be expanded into

(3.21)
$$\max_{(a_{i,j},\theta_{i,j})\in\Gamma}\left\{\frac{2}{h}U_{i,j}-\frac{a_{i,j}}{h}\,\mathcal{I}_hU|_{\mathbf{x}_{i,j}+\sqrt{h}(\mathbf{e}_z)_{i,j}}-\frac{a_{i,j}}{h}\,\mathcal{I}_hU|_{\mathbf{x}_{i,j}-\sqrt{h}(\mathbf{e}_z)_{i,j}}\right.$$
$$-\frac{1-a_{i,j}}{h}\,\mathcal{I}_hU|_{\mathbf{x}_{i,j}+\sqrt{h}(\mathbf{e}_w)_{i,j}}-\frac{1-a_{i,j}}{h}\,\mathcal{I}_hU|_{\mathbf{x}_{i,j}-\sqrt{h}(\mathbf{e}_w)_{i,j}}$$
$$\left.+2\sqrt{a_{i,j}(1-a_{i,j})f_{i,j}}\right\}=0.$$

We can further expand each bilinear interpolation term. For instance, if we denote the four neighbouring points around $\mathbf{x}_{i,j}+\sqrt{h}(\mathbf{e}_z)_{i,j}$ as $\mathbf{x}_{r,s}$, $\mathbf{x}_{r+1,s}$, $\mathbf{x}_{r,s+1}$ and $\mathbf{x}_{r+1,s+1}$, as shown in Figure 3.3 (right), then

(3.22)
$$\mathcal{I}_hU|_{\mathbf{x}_{i,j}+\sqrt{h}(\mathbf{e}_z)_{i,j}}=\omega_{r,s}U_{r,s}+\omega_{r+1,s}U_{r+1,s}+\omega_{r,s+1}U_{r,s+1}+\omega_{r+1,s+1}U_{r+1,s+1},$$

where $\omega_{r,s}$, $\omega_{r+1,s}$, $\omega_{r,s+1}$, $\omega_{r+1,s+1}$ are the associated bilinear interpolation weights, which are determined by the position of $\mathbf{x}_{i,j} + \sqrt{h}(\mathbf{e}_z)_{i,j}$. This shows explicitly that each bilinear interpolation term contains 4 unknown values. As a result, (3.21) has 17 unknown values. Once again, (3.17) and (3.18) hold.

We remark that the same analysis can be applied to the other cases, including:

Case 4. Condition (3.4) is satisfied at a grid point $\mathbf{x}_{i,j}$, either inside the computational domain or near the boundary. Narrow stencil discretization (3.6) with $disc = 2$ is applied.

Case 5. Neither (3.2) nor (3.4) is satisfied at a grid point $\mathbf{x}_{i,j}$ that is near the boundary. Wide stencil discretization (3.14) is applied, and stencil truncation is needed.

The general form of the discrete equations (3.15)-(3.16) can be further rewritten into a concise matrix form. In order to do this, we define $\mathbf{U} \in \mathbb{R}^{N^2\times 1}$, which is a vector of the unknowns arranged under the following lexicographic order,

$$\mathbf{U} \equiv (U_{1,1}, U_{2,1}, \cdots, U_{N,1}, U_{1,2}, \cdots\cdots, U_{N,N})^T. \tag{3.23}$$

Then the entire discrete system can be rewritten from (3.15)-(3.16) to:

$$\max_{(a,\theta)\in\Gamma} \{\mathbf{A}(a,\theta)\,\mathbf{U} - \mathbf{F}(a,\theta)\} = 0, \tag{3.24}$$

where $a \in \mathbb{R}^{N^2\times 1}$, $\theta \in \mathbb{R}^{N^2\times 1}$, $\mathbf{A}(a,\theta) \in \mathbb{R}^{N^2\times N^2}$ and $\mathbf{F}(a,\theta) \in \mathbb{R}^{N^2\times 1}$.

4. Solving the Nonlinear Discrete System.

4.1. Policy iteration. After setting up the complete nonlinear discrete system (3.15)-(3.16), or equivalently, (3.24), the next objective is to solve it. We note that given a control pair (a,θ), the nonlinear discrete system (3.24) is reduced to a linear one. In this section, we apply a fixed point iteration algorithm, called "policy iteration" [16, 13]. Policy iteration consists of two sub-steps. One is solving a maximization problem for the optimal control pair (a^*,θ^*). The other is solving a discrete linear system for the numerical solution $\mathbf{U}$ under a given control pair. The algorithm can be formulated as follows:

Algorithm: Policy iteration

Start with an initial guess of the solution $\mathbf{U}^{(0)}$.

For $k = 0, 1, ...$ until convergence

1. For all $\mathbf{x}_{i,j} \in \Omega$, solve for the optimal control pair $\left(a_{i,j}^{(k)}, \theta_{i,j}^{(k)}\right)$ under the current solution $\mathbf{U}^{(k)}$:

$$\left(a_{i,j}^{(k)}, \theta_{i,j}^{(k)}\right) = \underset{(a_{i,j},\theta_{i,j})\in\Gamma}{\arg\max}\ \mathcal{L}^h\left(\mathbf{x}_{i,j}; a_{i,j}, \theta_{i,j}; \mathbf{U}^{(k)}\right), \tag{4.1}$$

where we use a concise notation for the objective function (3.16) as follows:

$$\mathcal{L}^h\left(\mathbf{x}_{i,j}; a_{i,j}, \theta_{i,j}; \mathbf{U}\right) \equiv \mathcal{L}^h\left(\mathbf{x}_{i,j}; a_{i,j}, \theta_{i,j}; U_{i,j}, \{U_{p,q}|_{(p,q)\neq(i,j)}\}\right). \tag{4.2}$$

Meanwhile, obtain the residual $\mathbf{R}^{(k)} \in \mathbb{R}^{N^2\times 1}$, where each component is given by the value of the objective function

$$R_{i,j}^{(k)} \equiv \mathcal{L}^h\left(\mathbf{x}_{i,j}; a_{i,j}^{(k)}, \theta_{i,j}^{(k)}; \mathbf{U}^{(k)}\right). \tag{4.3}$$

2. If $\|\mathbf{R}^{(k)}\| \leq$ tolerance: break
Else
Solve the following linear system for the solution $\mathbf{U}^{(k+1)}$ under the current optimal control pair $(a^{(k)}, \theta^{(k)})$:

$$\mathbf{A}(a^{(k)}, \theta^{(k)})\, \mathbf{U}^{(k+1)} = \mathbf{F}(a^{(k)}, \theta^{(k)}) \qquad \Rightarrow \qquad \mathbf{U}^{(k+1)}. \tag{4.4}$$

End for

Final numerical solution: $\mathbf{U} = \mathbf{U}^{(k)}$.
Final optimal control pair: $(a^*, \theta^*) = (a^{(k)}, \theta^{(k)})$.

It is well-known that policy iteration is guaranteed to converge for any initial guess $\mathbf{U}^{(0)}$, if by applying a monotone discretization to an HJB equation, the resulting matrix $\mathbf{A}(a, \theta)$ is a strictly diagonally dominant M-matrix under all admissible controls[6]. However, the resulting matrix $\mathbf{A}(a, \theta)$ in (3.24) is instead a weakly chained diagonally dominant M-matrix[24]. It has not been proved until recently that the convergence of policy iteration is still guaranteed for any $\mathbf{U}^{(0)}$ for a weakly chained diagonally dominant M-matrix [2].

4.2. Implementation of policy iteration. In the following part, we focus on the practical implementation of the two sub-steps of the policy iteration. One sub-step is to solve the linear system under a given control pair; see (4.4). We note that for the $N^2 \times N^2$ matrix $\mathbf{A}(a, \theta)$, if narrow stencil discretization is applied at $\mathbf{x}_{i,j}$, the corresponding row has at most 7 non-zero elements and the band width is about N. As a comparison, if wide stencil discretization is applied at $\mathbf{x}_{i,j}$, the corresponding row has at most 17 non-zero elements and the band width is around $N\sqrt{N}$. Hence, maximal use of the narrow stencil discretization can speed up computation. Exact solver (complete LU factorization) has a high computational cost, and Krylov subspace methods, such as the GMRES with the incomplete LU preconditioner, are considered good choices.

The other sub-step of the policy iteration is to solve the optimization problem at each grid point $\mathbf{x}_{i,j}$; see (4.1). We remark that since in (3.14), the discretization of $(U_{zz})_{i,j}$ and $(U_{ww})_{i,j}$ depends on the control $\theta_{i,j}$, there is no simple closed-form formula to evaluate the optimal $\left(a_{i,j}^{(k)}, \theta_{i,j}^{(k)}\right)$ directly. In this case, one typical approach is to use bilinear search algorithm for the optimization problem. More specifically, we discretize the continuous admissible control set $\Gamma_{i,j} = [0,1] \times [-\frac{\pi}{4}, \frac{\pi}{4})^2$ into an $M \times M$ discrete set, denoted as $\Gamma_{i,j}^h$, compute the $M \times M$ values of the objective function $\mathcal{L}^h$ on $\Gamma_{i,j}^h$, and then find the global maximal value, which gives the optimal $\left(a_{i,j}^{(k)}, \theta_{i,j}^{(k)}\right)$. However, the computational cost of the bilinear search is $O(M^2)$. If we apply bilinear search on the entire computational domain Ω, which contains N^2 grid points, then the total computational cost is as high as $O(N^2 M^2)$. In addition, the discretization $\Gamma_{i,j} \to \Gamma_{i,j}^h$ introduces an additional truncation error.

In order to circumvent these issues, we consider dividing the continuous admissible

[2]The subscript "i,j" in $\Gamma_{i,j}$ highlights that we are considering the optimization problem at a grid point $\mathbf{x}_{i,j}$, or, we associate this grid point with an admissible control set $\Gamma_{i,j} = [0,1] \times [-\frac{\pi}{4}, \frac{\pi}{4})$, on which we solve the optimization problem for the optimal $(a_{i,j}^{(k)}, \theta_{i,j}^{(k)}) \in \Gamma_{i,j}$.

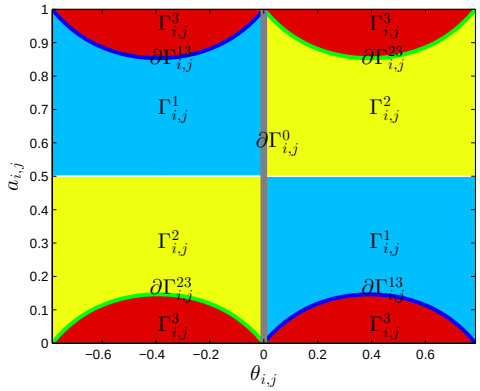

Region	Definition	Discretization	Algorithm for the optimization problem within each region	Cost of the optimization algorithm	Whether extra truncation error is introduced by the optimization algorithm
$\Gamma^1_{i,j}$	The region where Condition (3.2) is satisfied	Narrow stencil with $disc = 1$	Closed-form formula from first derivative test	$O(1)$	No
$\Gamma^2_{i,j}$	The region where Condition (3.4) is satisfied	Narrow stencil with $disc = 2$	Closed-form formula from first derivative test	$O(1)$	No
$\Gamma^3_{i,j}$	The region where neither (3.2) nor (3.4) is satisfied	Wide stencil	Linear search algorithm over a single control $\theta_{i,j} \in [-\frac{\pi}{4}, \frac{\pi}{4})$	$O(M)$	Yes
$\partial\Gamma^0_{i,j}$	The line $\theta_{i,j} = 0$	Narrow stencil with $disc = 1$ or $disc = 2$	Closed-form formula from first derivative test	$O(1)$	No
$\partial\Gamma^{13}_{i,j}$	The boundary between $\Gamma^1_{i,j}$ and $\Gamma^3_{i,j}$	Narrow stencil with $disc = 1$ or wide stencil	Linear search algorithm over a single control $\theta_{i,j} \in [-\frac{\pi}{4}, \frac{\pi}{4})$	$O(M)$	Yes
$\partial\Gamma^{23}_{i,j}$	The boundary between $\Gamma^2_{i,j}$ and $\Gamma^3_{i,j}$	Narrow stencil with $disc = 2$ or wide stencil	Linear search algorithm over a single control $\theta_{i,j} \in [-\frac{\pi}{4}, \frac{\pi}{4})$	$O(M)$	Yes

FIG. 4.1. *Division of the admissible control set* $\Gamma_{i,j} = [0,1] \times [-\frac{\pi}{4}, \frac{\pi}{4})$ *into regions. For each region, the characterization, discretization, optimization algorithm and the corresponding cost / truncation error of the optimization algorithm are listed.*

control set $\Gamma_{i,j} = [0,1] \times [-\frac{\pi}{4}, \frac{\pi}{4})$ into six regions, as shown in Figure 4.1[3]. The six regions are identified by whether a control pair $(a_{i,j}, \theta_{i,j})$ satisfies Condition (3.2), or Condition (3.4), or neither. Our approach is to find the optimal control within each region, and then find the global optimal control among the six regional optimal controls. This approach enables us to make full use of the analytical property of each region, and to improve the optimization algorithm within each region, and eventually

[3]It is unnecessary to consider the line $a_{i,j} = \frac{1}{2}$, since the objective function is a constant on this line. Also it is unnecessary to consider the line $\theta_{i,j} = \pm\frac{\pi}{4}$, since $\mathcal{L}_{a,\theta}\, u = \mathcal{L}_{1-a,\theta+\frac{\pi}{2}}\, u$ indicates that $\theta_{i,j} = \pm\frac{\pi}{4}$ is indeed an interior part of $\Gamma^1_{i,j}$ and $\Gamma^2_{i,j}$.

the entire admissible control set $\Gamma_{i,j}$.

Using our approach, the computational cost of solving the optimization problem on $\Gamma_{i,j}$ can be reduced from $O(M^2)$ to $O(M)$. In particular, the improvement of the optimization algorithm is significant on $\Gamma^1_{i,j} \cup \Gamma^2_{i,j} \cup \partial\Gamma^0_{i,j}$, where narrow stencil can be applied monotonically. In these narrow-stencil regions, we will see that closed-form formula for the optimal control is available, and discretization of $\Gamma^1_{i,j} \cup \Gamma^2_{i,j} \cup \partial\Gamma^0_{i,j}$ is no longer needed. This leads to two benefits. One is that the computational cost on $\Gamma^1_{i,j} \cup \Gamma^2_{i,j} \cup \partial\Gamma^0_{i,j}$ is reduced from $O(M^2)$ to $O(1)$. The other is that no truncation error is introduced by the optimization algorithm. In addition, we note that these narrow-stencil regions account for around 80% of the entire control set $\Gamma_{i,j}$, so our approach can make the the overall computation significantly more efficient.

The rest of the section explains how to solve each regional optimization problem effectively.

Region $\Gamma^1_{i,j}$. The region is defined where Condition (3.2) is satisfied. Equation (3.6) gives the objective function in $\Gamma^1_{i,j}$:

(4.5)
$$\begin{aligned}\mathcal{L}^h(a_{i,j},\theta_{i,j}) \quad &= -\alpha_{11}(a_{i,j},\theta_{i,j})(U_{xx})_{i,j} - 2\alpha_{12}(a_{i,j},\theta_{i,j})(U_{xy})^{(1)}_{i,j} \\ &\quad -\alpha_{22}(a_{i,j},\theta_{i,j})(U_{yy})_{i,j} + 2\sqrt{a_{i,j}(1-a_{i,j})f_{i,j}}, \quad (a_{i,j},\theta_{i,j}) \in \Gamma^1_{i,j},\end{aligned}$$

where we manifest the dependency of $\mathcal{L}^h$ on the control pair $(a_{i,j},\theta_{i,j})$ and suppress the other arguments. One can verify that this function is smooth in $(a_{i,j},\theta_{i,j})$, concave in $a_{i,j}$, and its stationary point in $\Gamma^1_{i,j}$ is unique, if it exists. This allows us to use first derivative test to find the optimal control pair in $\Gamma^1_{i,j}$:

$$\begin{aligned}\theta^{\Gamma^1}_{i,j} = \frac{1}{2}\arctan\frac{2(U_{xy})^{(1)}_{i,j}}{(U_{yy})_{i,j}-(U_{xx})_{i,j}}, \quad a^{\Gamma^1}_{i,j} = \frac{1}{2}\left(1-\frac{\lambda}{\sqrt{4f_{i,j}+\lambda^2}}\right), \\ \text{where } \lambda = [(U_{xx})_{i,j}-(U_{yy})_{i,j}]\cos 2\theta^{\Gamma^1}_{i,j} - 2(U_{xy})^{(1)}_{i,j}\sin 2\theta^{\Gamma^1}_{i,j}.\end{aligned} \tag{4.6}$$

If $(a^{\Gamma^1}_{i,j},\theta^{\Gamma^1}_{i,j}) \in \Gamma^1_{i,j}$, then the maximum in $\Gamma^1_{i,j}$ must occur at $(a^{\Gamma^1}_{i,j},\theta^{\Gamma^1}_{i,j})$. Otherwise, the maximum must occur on the boundary of $\Gamma^1_{i,j}$, or more specifically, either $\partial\Gamma^0_{i,j}$ or $\partial\Gamma^{13}_{i,j}$, which will be investigated separately.

Region $\Gamma^2_{i,j}$. The region is defined where Condition (3.4) is satisfied. The procedure for solving the optimization problem in $\Gamma^2_{i,j}$ is the same as $\Gamma^1_{i,j}$, except that $(U_{xy})^{(1)}_{i,j}$ in (4.5), (4.6) is replaced by $(U_{xy})^{(2)}_{i,j}$.

Region $\partial\Gamma^0_{i,j}$. This is the line $\theta_{i,j}=0$ which separates Region $\Gamma^1_{i,j}$ and $\Gamma^2_{i,j}$. The objective function in $\partial\Gamma^0_{i,j}$ can be extracted from (3.6):

$$\begin{aligned}\mathcal{L}^h(a_{i,j}) = -a_{i,j}(U_{xx})_{i,j} - (1-a_{i,j})(U_{yy})_{i,j} + 2\sqrt{a_{i,j}(1-a_{i,j})f_{i,j}}, \\ (a_{i,j},\theta_{i,j}) = (a_{i,j},0) \in \partial\Gamma^0_{i,j}.\end{aligned} \tag{4.7}$$

The first derivative test yields the optimal control pair in $\partial\Gamma^0_{i,j}$:

$$\begin{aligned}\theta^{\partial\Gamma^0}_{i,j} = 0, \quad a^{\partial\Gamma^0}_{i,j} = \frac{1}{2}\left(1-\frac{\lambda}{\sqrt{4f_{i,j}+\lambda^2}}\right), \\ \text{where } \lambda = (U_{xx})_{i,j} - (U_{yy})_{i,j}.\end{aligned} \tag{4.8}$$

Region $\partial\Gamma^{13}_{i,j}$. This is the boundary between Region $\Gamma^1_{i,j}$ and $\Gamma^3_{i,j}$. $\partial\Gamma^{13}_{i,j}$ can be seen as the following two-section parametrized curve:

$$a^{\partial\Gamma^{13}}_{i,j}(\theta_{i,j}) = \begin{cases} \mathcal{C}^+(\theta_{i,j}), & \theta_{i,j} \in [-\frac{\pi}{4}, 0), \\ \mathcal{C}^-(\theta_{i,j}), & \theta_{i,j} \in [0, \frac{\pi}{4}), \end{cases} \tag{4.9}$$

where

$$\mathcal{C}^{\pm}(\theta_{i,j}) \equiv \frac{1}{2}\left(1 \pm \frac{1}{\sqrt{2}\sin 2(|\theta_{i,j}| + \frac{\pi}{4})}\right), \quad \theta_{i,j} \in [-\frac{\pi}{4}, \frac{\pi}{4}). \tag{4.10}$$

We note that (4.9) can be derived from Condition (3.2).

The objective function on $\partial\Gamma^{13}_{i,j}$ is the same as (4.5), except that $a_{i,j}$ is now a function of $\theta_{i,j}$, defined by the parametrized curve (4.9). As a result, the objective function (4.5) becomes a function of the single control variable $\theta_{i,j}$:

$$\mathcal{L}^h(a^{\partial\Gamma^{13}}_{i,j}(\theta_{i,j}), \theta_{i,j}), \qquad \theta_{i,j} \in [-\frac{\pi}{4}, \frac{\pi}{4}). \tag{4.11}$$

A linear search can be performed for the maximum of the objective function over the single control variable $\theta_{i,j} \in [-\frac{\pi}{4}, \frac{\pi}{4})$.

Region $\partial\Gamma^{23}_{i,j}$. This is the boundary between Region $\Gamma^2_{i,j}$ and $\Gamma^3_{i,j}$. The treatment of the optimization problem in $\partial\Gamma^{23}_{i,j}$ is similar to $\partial\Gamma^{13}_{i,j}$, if we note that $\partial\Gamma^{23}_{i,j}$ can be parametrized by

$$a^{\partial\Gamma^{23}}_{i,j}(\theta_{i,j}) = \begin{cases} \mathcal{C}^-(\theta_{i,j}), & \theta_{i,j} \in [-\frac{\pi}{4}, 0), \\ \mathcal{C}^+(\theta_{i,j}), & \theta_{i,j} \in [0, \frac{\pi}{4}). \end{cases} \tag{4.12}$$

This can be derived from Condition (3.4).

Region $\Gamma^3_{i,j}$. The region is defined where neither (3.2) nor (3.4) is satisfied. The wide stencil discretization (3.14) is applied in $\Gamma^3_{i,j}$. Accordingly, the objective function is given by

$$\mathcal{L}^h(a_{i,j}, \theta_{i,j}) = -a_{i,j}\,(U_{zz})_{i,j} - (1 - a_{i,j})\,(U_{ww})_{i,j} + 2\sqrt{a_{i,j}\,(1 - a_{i,j})\,f_{i,j}}, \quad (a_{i,j}, \theta_{i,j}) \in \Gamma^3_{i,j}. \tag{4.13}$$

One can prove that the optimal control pair $(a^{\Gamma^3}_{i,j}, \theta^{\Gamma^3}_{i,j}) \in \Gamma^3_{i,j}$ must sit on the following parametrized curve

$$a^{\Gamma^3}_{i,j}(\theta_{i,j}) = \begin{cases} \mathcal{C}^\lambda(\theta_{i,j}), & \text{if } \mathcal{C}^\lambda(\theta_{i,j}) \le \mathcal{C}^-(\theta_{i,j}) \text{ or } \mathcal{C}^\lambda(\theta_{i,j}) \ge \mathcal{C}^+(\theta_{i,j}), \\ \mathcal{C}^-(\theta_{i,j}), & \text{if } \mathcal{C}^-(\theta_{i,j}) \le \mathcal{C}^\lambda(\theta_{i,j}) \le \frac{1}{2}, \\ \mathcal{C}^+(\theta_{i,j}), & \text{if } \frac{1}{2} \le \mathcal{C}^\lambda(\theta_{i,j}) \le \mathcal{C}^+(\theta_{i,j}). \end{cases} \tag{4.14}$$

Here

$$\mathcal{C}^\lambda(\theta_{i,j}) = \frac{1}{2}\left(1 - \frac{\lambda}{\sqrt{4f_{i,j} + \lambda^2}}\right), \quad \text{where } \lambda = (U_{zz})_{i,j} - (U_{ww})_{i,j}, \tag{4.15}$$

is given by the first derivative test of (4.13). We note that the directions of z and w depend on $\theta_{i,j}$.

This motivates us to perform once again a linear search for the maximum of the objective function

$$\mathcal{L}^h(a_{i,j}^{\Gamma^3}(\theta_{i,j}), \theta_{i,j}), \qquad \theta_{i,j} \in [-\frac{\pi}{4}, \frac{\pi}{4}), \tag{4.16}$$

where $a_{i,j}$ has been parametrized to $a_{i,j}^{\Gamma^3}(\theta_{i,j})$ under (4.14).

Once we obtain the six regional optimal control pairs

$$\begin{array}{lll} (a_{i,j}^{\Gamma^1}, \theta_{i,j}^{\Gamma^1}), & (a_{i,j}^{\Gamma^2}, \theta_{i,j}^{\Gamma^2}), & (a_{i,j}^{\Gamma^3}, \theta_{i,j}^{\Gamma^3}), \\ (a_{i,j}^{\partial\Gamma^0}, \theta_{i,j}^{\partial\Gamma^0}), & (a_{i,j}^{\partial\Gamma^{13}}, \theta_{i,j}^{\partial\Gamma^{13}}), & (a_{i,j}^{\partial\Gamma^{23}}, \theta_{i,j}^{\partial\Gamma^{23}}), \end{array} \tag{4.17}$$

and their corresponding objective function values, we search within these six values for the global maximum on $\Gamma_{i,j}$. This step is cheap and straightforward.

To summarize Section 4, we implement policy iteration to solve the nonlinear discrete system (3.15)-(3.16), or equivalently, (3.24), which is guaranteed to converge. Policy iteration contains two sub-steps: (1) solving an optimization problem for the optimal control pair, and (2) solving a linear system under the fixed control pair. Step (1) using bilinear search turns out to be time consuming and inaccurate. To improve both efficiency and accuracy, we divide the admissible control set $\Gamma_{i,j}$ into several regions, solve optimal problem within each region effectively, and then solve the global optimization problem with only six elements to search. The final computational cost of solving the optimization problem on $\Gamma_{i,j}$ is decreased from $O(M^2)$ to $O(M)$.

5. Convergence Analysis. As proved by Barles and Souganidis [3], there are three sufficient conditions for the numerical scheme of a nonlinear PDE to converge in the viscosity sense. In this section, we will prove that our numerical scheme does fulfill all the three requirements and is therefore guaranteed to converge to the viscosity solution of (1.1).

5.1. Consistency. One sufficient condition for convergence is consistency. Intuitively, consistency claims that the discretized equation of a PDE should be close to the continuous PDE. In particular, when $h \to 0$, the discretized equation should converge to the PDE. The main result of this subsection is to prove that our numerical scheme is consistent in the viscosity sense:

LEMMA 5.1 (Consistency). *For the Monge-Ampère equation $\mathcal{F}\left(\mathbf{x}, D^2u(\mathbf{x})\right) = 0$, the numerical scheme $\mathcal{F}^h\left(\mathbf{x}_{i,j}, U_{i,j}, \{U_{p,q}|_{(p,q)\neq(i,j)}\}\right) = 0$, given in (3.15)-(3.16), is consistent in the viscosity sense. More specifically, for any function $\varphi(\mathbf{x}) \in C^\infty(\Omega)$ with $\varphi_{i,j} = \varphi(\mathbf{x}_{i,j})$, for any $\hat{\mathbf{x}} \in \Omega$, and for h and ξ that are arbitrary small constants independent of $\mathbf{x}$, we have*

$$\limsup_{\substack{h\to 0 \\ \xi\to 0 \\ \mathbf{x}_{i,j}\to\hat{\mathbf{x}}}} \mathcal{F}^h\left(\mathbf{x}_{i,j}, \varphi_{i,j}+\xi, \{\varphi_{p,q}+\xi|_{(p,q)\neq(i,j)}\}\right) \le \mathcal{F}^*(\hat{\mathbf{x}}, D^2\varphi(\hat{\mathbf{x}})), \tag{5.1}$$

and

$$\liminf_{\substack{h\to 0 \\ \xi\to 0 \\ \mathbf{x}_{i,j}\to\hat{\mathbf{x}}}} \mathcal{F}^h\left(\mathbf{x}_{i,j}, \varphi_{i,j}+\xi, \{\varphi_{p,q}+\xi|_{(p,q)\neq(i,j)}\}\right) \ge \mathcal{F}_*(\hat{\mathbf{x}}, D^2\varphi(\hat{\mathbf{x}})), \tag{5.2}$$

where $\mathcal{F}^*$ and $\mathcal{F}_*$ are defined in (2.3).

In practise, we prove a sufficient condition for consistency, called local consistency, as follows:

LEMMA 5.2 (Local consistency). *Under the assumptions in Lemma 5.1, we have*

(5.3)
$$\begin{aligned}&\mathcal{F}\left(\mathbf{x}_{i,j}, D^2\varphi(\mathbf{x}_{i,j})\right) - \mathcal{F}^h\left(\mathbf{x}_{i,j}, \varphi_{i,j}+\xi, \{\varphi_{p,q}+\xi|_{(p,q)\neq(i,j)}\}\right)\\ &= \begin{cases} O(h^2)+O(\xi), & \textit{narrow stencil},\\ O(h)+O(\xi), & \textit{wide stencil, with all the 4 wide stencil points } \in \Omega,\\ O(\sqrt{h})+O(\xi), & \textit{wide stencil, otherwise},\end{cases}\end{aligned}$$

or equivalently,

$$\begin{aligned}&\mathcal{F}\left(\mathbf{x}_{i,j}, D^2\varphi(\mathbf{x}_{i,j})\right) - \mathcal{F}^h\left(\mathbf{x}_{i,j}, \varphi_{i,j}, \{\varphi_{p,q}|_{(p,q)\neq(i,j)}\}\right)\\ &= \begin{cases} O(h^2), & \textit{narrow stencil},\\ O(h), & \textit{wide stencil, with all the 4 wide stencil points } \in \Omega,\\ O(\sqrt{h}), & \textit{wide stencil, otherwise.}\end{cases}\end{aligned} \tag{5.4}$$

Proof. The equivalence between (5.3) and (5.4) can be easily verified if we substitute φ by $\varphi+\xi$ in the following proof, so we will only prove (5.4). In the proof, we use the smooth test function $\varphi \in C^\infty(\Omega)$.

Case 1: Truncation error of narrow stencil discretization. Suppose narrow stencil discretization is applied at $\mathbf{x}_{i,j}$. Taylor expansion can prove that narrow stencil discretization is second order accurate. More explicitly, under the discretization (3.1), the truncation error of φ_{xx} can be expressed as

$$\varphi_{xx}(\mathbf{x}_{i,j}) - (\varphi^h_{xx})_{i,j} = O(h^2), \tag{5.5}$$

where

$$(\varphi^h_{xx})_{i,j} \equiv \frac{1}{h^2}(\varphi_{i+1,j} - 2\varphi_{i,j} + \varphi_{i-1,j}). \tag{5.6}$$

The same conclusion holds for φ_{yy} under the discretization (3.1), and φ_{xy} under the discretization (3.3) and (3.5).

Following this conclusion, one can show that the local truncation error of the finite difference scheme at $\mathbf{x}_{i,j}$ is

$$\mathcal{F}\left(\mathbf{x}_{i,j}, D^2\varphi(\mathbf{x}_{i,j})\right) - \mathcal{F}^h\left(\mathbf{x}_{i,j}, \varphi_{i,j}, \{\varphi_{p,q}|_{(p,q)\neq(i,j)}\}\right) = O(h^2), \tag{5.7}$$

since

(5.8)
$$\begin{aligned}&\left|\ \mathcal{F}\left(\mathbf{x}_{i,j}, D^2\varphi(\mathbf{x}_{i,j})\right) - \mathcal{F}^h\left(\mathbf{x}_{i,j}, \varphi_{i,j}, \{\varphi_{p,q}|_{(p,q)\neq(i,j)}\}\right)\ \right|\\ =&\Bigg| \max_{(a_{i,j},\theta_{i,j})\in\Gamma}\Big\{ -\alpha_{11}(a_{i,j},\theta_{i,j})\varphi_{xx}(\mathbf{x}_{i,j}) - 2\alpha_{12}(a_{i,j},\theta_{i,j})\varphi_{xy}(\mathbf{x}_{i,j})\\ &\qquad -\alpha_{22}(a_{i,j},\theta_{i,j})\varphi_{yy}(\mathbf{x}_{i,j}) + 2\sqrt{a_{i,j}(1-a_{i,j})f_{i,j}}\Big\}\\ &- \max_{(a_{i,j},\theta_{i,j})\in\Gamma}\Big\{ -\alpha_{11}(a_{i,j},\theta_{i,j})(\varphi^h_{xx})_{i,j} - 2\alpha_{12}(a_{i,j},\theta_{i,j})(\varphi^h_{xy})_{i,j}\\ &\qquad -\alpha_{22}(a_{i,j},\theta_{i,j})(\varphi^h_{yy})_{i,j} + 2\sqrt{a_{i,j}(1-a_{i,j})f_{i,j}}\Big\}\ \Bigg|\end{aligned}$$

$$\leq \max_{(a_{i,j},\theta_{i,j})\in\Gamma} \Big| \alpha_{11}(a_{i,j},\theta_{i,j}) \left((\varphi^h_{xx})_{i,j} - \varphi_{xx}(\mathbf{x}_{i,j})\right) + 2\alpha_{12}(a_{i,j},\theta_{i,j}) \left((\varphi^h_{xy})_{i,j} - \varphi_{xy}(\mathbf{x}_{i,j})\right) + \alpha_{22}(a_{i,j},\theta_{i,j}) \left((\varphi^h_{yy})_{i,j} - \varphi_{yy}(\mathbf{x}_{i,j})\right)\Big| = O(h^2).$$

The second inequality comes from $\left|\max_x f(x) - \max_x g(x)\right| \leq \max_x |f(x) - g(x)|$.

Case 2: Truncation error of wide stencil discretization. Suppose wide stencil discretization is applied at $\mathbf{x}_{i,j}$. We focus on the truncation error of φ_{zz} only and analyze three cases. The first case is that both the stencil points of φ_{zz} are in the computational domain. The discretization is given by (3.11). The truncation error of φ_{zz} is $O(h)$, since

(5.9)
$$\begin{aligned} & \varphi_{zz}(\mathbf{x}_{i,j}) - \frac{1}{h}\left[\mathcal{I}_h\varphi|_{\mathbf{x}_{i,j}+\sqrt{h}(\mathbf{e}_z)_{i,j}} - 2\varphi(\mathbf{x}_{i,j}) + \mathcal{I}_h\varphi|_{\mathbf{x}_{i,j}-\sqrt{h}(\mathbf{e}_z)_{i,j}}\right] \\ = \;& \varphi_{zz}(\mathbf{x}_{i,j}) - \frac{1}{h}\left[\varphi(\mathbf{x}_{i,j}+\sqrt{h}(\mathbf{e}_z)_{i,j}) - 2\varphi(\mathbf{x}_{i,j}) + \varphi(\mathbf{x}_{i,j}-\sqrt{h}(\mathbf{e}_z)_{i,j}) + O(h^2)\right] \\ = \;& O(h) + O(h) = O(h). \end{aligned}$$

From the first to the second line we have used the fact that the truncation error of the bilinear interpolation is $O(h^2)$, and from the second to the last line we have used the quadratic truncation error of central differencing with respect to the wide stencil length $\sqrt{h}$, which is $O\left((\sqrt{h})^2\right) = O(h)$. As a comparison, if we choose narrow stencil length h and work through the same algebra, the truncation error will be instead $O(1)$, which is no longer consistent. This justifies the choice of the wide stencil.

Now we consider another case, where one of the stencil points of φ_{zz} falls outside the computational domain and is thus relocated. Without loss of generality, let us assume that $\mathbf{x}_{i,j} + \eta_1(\mathbf{e}_z)_{i,j} \in \partial\Omega$ is the relocated point. The discretization follows (3.12). The truncation error of φ_{zz} is $O(\sqrt{h})$, since

(5.10)
$$\begin{aligned} & \varphi_{zz}(\mathbf{x}_{i,j}) - \frac{\frac{\varphi(\mathbf{x}_{i,j}+\eta_1(\mathbf{e}_z)_{i,j})-\varphi(\mathbf{x}_{i,j})}{\eta_1} - \frac{\varphi(\mathbf{x}_{i,j}) - \mathcal{I}_h\varphi|_{\mathbf{x}_{i,j}-\sqrt{h}(\mathbf{e}_z)_{i,j}}}{\sqrt{h}}}{\frac{\eta_1+\sqrt{h}}{2}} \\ = \;& \varphi_{zz}(\mathbf{x}_{i,j}) - \frac{\frac{\varphi(\mathbf{x}_{i,j}+\eta_1(\mathbf{e}_z)_{i,j})-\varphi(\mathbf{x}_{i,j})}{\eta_1} - \frac{\varphi(\mathbf{x}_{i,j})-\varphi(\mathbf{x}_{i,j}-\sqrt{h}(\mathbf{e}_z)_{i,j})}{\sqrt{h}}}{\frac{\eta_1+\sqrt{h}}{2}} + O\left(\frac{h^2}{\sqrt{h}\frac{\eta_1+\sqrt{h}}{2}}\right) \\ = \;& O(\sqrt{h}-\eta_1) + O\left(\frac{h^2}{\sqrt{h}\frac{\eta_1+\sqrt{h}}{2}}\right) = O(\sqrt{h}). \end{aligned}$$

We are yet to investigate the last case, where $\mathbf{x}_{i,j} + \eta_1(\mathbf{e}_z)_{i,j} \in \partial\Omega$ and $\mathbf{x}_{i,j} - \eta_2(\mathbf{e}_z)_{i,j} \in \partial\Omega$ are both relocated points. The discretization is given by (3.13). The truncation error of φ_{zz} is again $O(\sqrt{h})$, since

(5.11)
$$\varphi_{zz}(\mathbf{x}_{i,j}) - \frac{\frac{\varphi(\mathbf{x}_{i,j}+\eta_1(\mathbf{e}_z)_{i,j})-\varphi(\mathbf{x}_{i,j})}{\eta_1} - \frac{\varphi(\mathbf{x}_{i,j})-\varphi(\mathbf{x}_{i,j}-\eta_2(\mathbf{e}_z)_{i,j})}{\eta_2}}{\frac{\eta_1+\eta_2}{2}} = O(\eta_2-\eta_1) = O(\sqrt{h}).$$

Hence, by the same argument as (5.8), one can show that the local truncation error of the finite difference scheme at $\mathbf{x}_{i,j}$, where the wide stencil discretization is

applied, is given by

$$\begin{aligned}&\mathcal{F}\left(\mathbf{x}_{i,j}, D^2\varphi(\mathbf{x}_{i,j})\right) - \mathcal{F}^h\left(\mathbf{x}_{i,j}, \varphi_{i,j}, \{\varphi_{p,q}|_{(p,q)\neq(i,j)}\}\right)\\ &= \begin{cases} O(h), & \text{wide stencil, with all the 4 wide stencil points } \in \Omega,\\ O(\sqrt{h}), & \text{wide stencil, otherwise.}\end{cases}\end{aligned} \tag{5.12}$$

Finally, we note that the previous proof has assumed that the optimal control pair is solved exactly, or does not introduce additional truncation error. In Section 4, we have mentioned that the optimal control pair under the wide stencil discretization introduces truncation error. In particular, if we choose $M = O(N)$, and apply linear search, then $O(h)$ truncation error is introduced. See [26] for a proof. As a result, (5.12) holds. ∎

5.2. Stability. Another condition for convergence is stability, which means that the discrete system has a bounded solution $\mathbf{U}$. Stability condition is very closely related to the matrix $\mathbf{A}(a,\theta)$ in (3.24) being an M-matrix[23], which will be proved in this section.

Definition 5.3 (Weakly chained diagonally dominant (WCDD) L-matrix). *An $n \times n$ matrix $\mathbf{A}$ is a WCDD L-matrix if*

1. $\mathbf{A}$ *is an L-matrix:* $\mathbf{A}_{ii} > 0$ *for all* i, *and* $\mathbf{A}_{ij} \leq 0$ *for all* $i \neq j$.
2. $\mathbf{A}$ *is weakly diagonally dominant:* $|\mathbf{A}_{ii}| \geq \sum_{j\neq i} |\mathbf{A}_{ij}|$.
3. $\mathbf{A}$ *has the following connectivity property: Let* $\mathcal{G}(\mathbf{A}) = \left\{ i \,\middle|\, |\mathbf{A}_{ii}| > \sum_{j\neq i} |\mathbf{A}_{ij}| \right\}$ $\neq \emptyset$ *be the set of rows where strict inequality is achieved. For any* $i \notin \mathcal{G}(\mathbf{A})$, *there exists a sequence* $i_1, i_2, \cdots, i_k$ *with* $\mathbf{A}_{i_r,i_{r+1}} \neq 0,\ 0 \leq r \leq k-1$, *such that* $i_0 = i$ *and* $i_k \in \mathcal{G}(\mathbf{A})$.

We remark on the connectivity property. It is equivalent of saying that if the matrix $\mathbf{A}$ is represented by a graph[23], for any node where the corresponding row is weakly diagonally dominant, there always exists a path to a node where the corresponding row is strongly diagonally dominant.

Lemma 5.4. *A WCDD L-matrix $\mathbf{A}$ is an M-matrix. This implies that $\mathbf{A}$ is non-singular and $\|\mathbf{A}^{-1}\|_\infty$ is bounded.*

Proof. We refer the readers to [24, 2]. [24] also derives a formula for the upper bound of $\|\mathbf{A}^{-1}\|_\infty$. ∎

Lemma 5.5. *The matrix $\mathbf{A}(a,\theta)$, defined in (3.24), is a WCDD L-matrix, and hence an M-matrix, under the set of admissible controls $(a,\theta) \in \Gamma$.*

Proof. Our goal is to verify that $\mathbf{A}(a,\theta)$ satisfies the three conditions in Definition 5.3. The L-matrix condition and the weakly diagonal dominance condition are essentially (3.17) and (3.18). These two conditions have been checked for the particular cases in Section 3.3. Using the same argument, one can extend the validity of the L-matrix condition (3.17) and the weakly diagonal dominance condition (3.18) to the general discrete equation (3.15)-(3.16). We remark that the strictly diagonally dominant rows correspond to the grid points near the boundary $\partial\Omega$, while the weakly diagonally dominant rows correspond to those inside the computation domain Ω.

The connectivity property of the discretization (3.15)-(3.16) is yet to be verified. For the grid points $\mathbf{x}_{i,j}$ that are near the boundary, the lexicographical index satisfies $N(i-1)+j \in \mathcal{G}(\mathbf{A})$. For those points that are inside the computational domain, or $N(i-1)+j \notin \mathcal{G}(\mathbf{A})$, there must exist non-zero entries $\mathbf{A}_{N(i-1)+j,N(i'-1)+j'} \neq 0$,

where $i' \geq i$, $j' \geq j$, with at lease one strict inequality satisfied. Hence, given any $\mathbf{x}_{i_0,j_0}$, where $N(i_0-1)+j_0 \notin \mathcal{G}(\mathbf{A})$, there exist monotonically increasing sequences $i_0 \leq i_1 \leq ... \leq i_k \leq N$ and $j_0 \leq j_1 \leq ... \leq j_k \leq N$, such that $N(i_k-1)+j_k \in \mathcal{G}(\mathbf{A})$. ∎

LEMMA 5.6 (Stability). *Given that under all admissible controls, $\mathbf{A}(a,\theta)$ in (3.24) is a WCDD L-matrix (which is also an M-matrix) and $\|\mathbf{F}(a,\theta)\|_\infty$ is bounded, the discrete system (3.24) has a unique solution $\mathbf{U}$, and $\|\mathbf{U}\|_\infty$ is bounded.*

Proof. See [18]. To sketch the proof, since $\mathbf{A}(a,\theta)$ is an M-matrix under all admissible controls, by Lemma 5.4, it is invertible and $\|\mathbf{A}(a,\theta)^{-1}\|_\infty$ is bounded. Hence $\|\mathbf{U}\|_\infty \leq \|\mathbf{A}(a,\theta)^{-1}\|_\infty \|\mathbf{F}(a,\theta)\|_\infty$ is bounded. ∎

5.3. Monotonicity. For nonlinear PDEs, monotonicity is another sufficient condition for convergence in the viscosity sense. Monotonicity means that given the discretization scheme at a grid point $\mathbf{x}_{i,j}$, the unknown $U_{i,j}$ must be a non-decreasing function of the unknowns at the other points $\{U_{p,q}|_{(p,q)\neq(i,j)}\}$. The monotonicity of our numerical scheme (3.15)-(3.16) is inherited from the property (3.17).

LEMMA 5.7 (Monotonicity). *The finite difference discretization*

$$\mathcal{F}^h\left(\mathbf{x}_{i,j}, U_{i,j}, \{U_{p,q}|_{(p,q)\neq(i,j)}\}\right) = 0,$$

given in (3.15)-(3.16), is monotone. More specifically, for all $\mathbf{U} \leq \mathbf{V}$, we have

$$\begin{aligned} &\mathcal{F}^h\left(\mathbf{x}_{i,j}, U_{i,j}, \{U_{p,q}|_{(p,q)\neq(i,j)}\}\right) \leq \mathcal{F}^h\left(\mathbf{x}_{i,j}, V_{i,j}, \{U_{p,q}|_{(p,q)\neq(i,j)}\}\right), \\ &\mathcal{F}^h\left(\mathbf{x}_{i,j}, U_{i,j}, \{U_{p,q}|_{(p,q)\neq(i,j)}\}\right) \geq \mathcal{F}^h\left(\mathbf{x}_{i,j}, U_{i,j}, \{V_{p,q}|_{(p,q)\neq(i,j)}\}\right). \end{aligned} \tag{5.13}$$

Proof. The proof follows [13]. Our goal is to verify the monotonicity condition (5.13). Without loss of generality, let us analyze one example: $\mathbf{U} \leq \mathbf{V}$, with $V_{r,s} = U_{r,s} + \epsilon$, $\epsilon \geq 0$, $(r,s) \neq (i,j)$, and $\{V_{p,q}\} = \{U_{p,q}\}$, $\forall (p,q) \neq (i,j)$ or (r,s).

$$\begin{aligned} &\mathcal{F}^h\left(\mathbf{x}_{i,j}, U_{i,j}, \{U_{p,q}|_{(p,q)\neq(i,j)}\}\right) - \mathcal{F}^h\left(\mathbf{x}_{i,j}, U_{i,j}, \{V_{p,q}|_{(p,q)\neq(i,j)}\}\right) \\ &= \max_{(a_{i,j},\theta_{i,j})\in\Gamma} \Big\{ A_{i,j}(a_{i,j},\theta_{i,j})\, U_{i,j} \;-\; A_{r,s}(a_{i,j},\theta_{i,j})\, U_{r,s} \\ &\qquad\qquad - \sum_{\substack{(p,q)\neq(i,j)\\(p,q)\neq(r,s)}} A_{p,q}(a_{i,j},\theta_{i,j})\, U_{p,q} \;- F_{i,j}(a_{i,j},\theta_{i,j}) \Big\} \\ &- \max_{(a_{i,j},\theta_{i,j})\in\Gamma} \Big\{ A_{i,j}(a_{i,j},\theta_{i,j})\, U_{i,j} \;-\; A_{r,s}(a_{i,j},\theta_{i,j})\, (U_{r,s}+\epsilon) \\ &\qquad\qquad - \sum_{\substack{(p,q)\neq(i,j)\\(p,q)\neq(r,s)}} A_{p,q}(a_{i,j},\theta_{i,j})\, U_{p,q} \;- F_{i,j}(a_{i,j},\theta_{i,j}) \Big\} \\ &\geq \epsilon \min_{(a_{i,j},\theta_{i,j})\in\Gamma} A_{r,s}(a_{i,j},\theta_{i,j}) \;\geq\; 0, \end{aligned}$$

where we have used the fact that $A_{r,s}(a_{i,j},\theta_{i,j}) \geq 0$ under all admissible controls and $\max_x f(x) - \max_x g(x) \geq \min_x [f(x) - g(x)]$. Hence, $\mathcal{F}^h$ is monotone. ∎

5.4. Convergence of the numerical solution to the viscosity solution. Once consistency, stability and monotonicity are proved, the Barles-Souganidis theorem [3] guarantees the convergence of the numerical solution to the viscosity solution.

THEOREM 5.8 (Barles-Souganidis theorem). *Given that the finite difference discretization (3.15)-(3.16) satisfies consistency, stability and monotonicity, it converges to the viscosity solution of the Dirichlet problem (1.1).*

Proof. See Barles and Souganidis's proof in [3]. ∎

6. Numerical Results. In this section, we will present numerical results for the Monge-Ampère equation using our mixed narrow/wide stencil method. These numerical results show that the mixed narrow/wide stencil method can achieve second order convergence rate for smooth viscosity solutions, and up to order one convergence rate for non-smooth viscosity solutions. The examples we consider in this section come from [14, 4]. We choose the tolerance of residual for the policy iteration to be 10^{-6}, and the initial guess of the numerical solution to be the solution of

$$\begin{aligned} u_{xx} + u_{yy} &= 2\sqrt{f}, && \text{in } \Omega, \\ u &= g, && \text{on } \partial\Omega, \end{aligned} \tag{6.1}$$

which corresponds to the solution of (2.9) with $a = \frac{1}{2}$ and arbitrary θ. We choose the grid size $N^2 = 32^2, 64^2, \cdots, 512^2$, and define the numerical convergence rate as

$$\log_2 \frac{\|u - \mathbf{U}_{N/2}\|}{\|u - \mathbf{U}_N\|}, \tag{6.2}$$

where $\mathbf{U}_N$ is the numerical solution on an $N \times N$ grid.

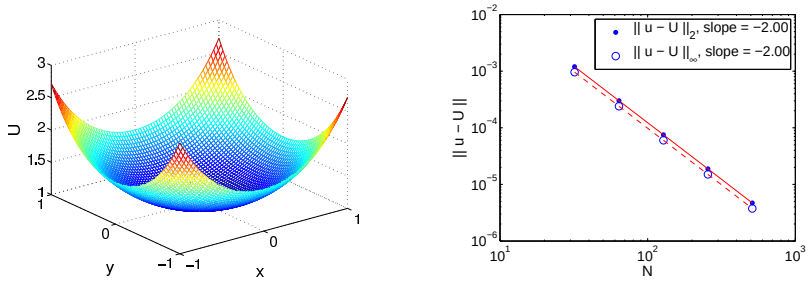

FIG. 6.1. *Example 1: Mixed narrow/wide stencil. The exact solution is* $u(x,y) = e^{\frac{1}{2}(x^2+y^2)}$. *(1) Numerical solution. (2) Norms of the error* $\|u - \mathbf{U}\|$. *The convergence rates, indicated by the slopes, are* $O(h^2)$ *in both* L_2 *and* L_∞ *norms.*

N	$\|u - \mathbf{U}\|_2$	Numerical convergence rate	$\|u - \mathbf{U}\|_\infty$	Numerical convergence rate	Number of policy iterations
32	1.201×10^{-3}		9.598×10^{-4}		4
64	3.009×10^{-4}	2.00	2.404×10^{-4}	2.00	4
128	7.526×10^{-5}	2.00	6.013×10^{-5}	2.00	4
256	1.882×10^{-5}	2.00	1.504×10^{-5}	2.00	4
512	4.705×10^{-6}	2.00	3.759×10^{-6}	2.00	4

TABLE 6.1

Example 1: Mixed narrow/wide stencil. The exact solution is $u(x,y) = e^{\frac{1}{2}(x^2+y^2)}$. *The convergence rates in both* L_2 *and* L_∞ *norms are* $O(h^2)$.

Example 1. Start with

$$f(x,y) = (1+x^2+y^2)e^{x^2+y^2}, \qquad g(x,y) = e^{\frac{1}{2}(x^2+y^2)}, \qquad \Omega = [-1,1]\times[-1,1], \tag{6.3}$$

where the exact solution

$$u(x,y) = e^{\frac{1}{2}(x^2+y^2)} \tag{6.4}$$

is smooth. For this example, it turns out that narrow stencil discretization can be applied on the entire computational domain and still results in a monotone scheme, since the optimal control pair (a^*, θ^*) at every grid point is inside the narrow stencil region $\Gamma^1 \cup \Gamma^2 \cup \partial\Gamma^0$. Consequentially, the numerical solution converges at the optimal theoretical convergence rate $O(h^2)$; see Figure 6.1 and Table 6.1. We observe that the computation is efficient, in the sense that the number of policy iterations remains a small constant 4 as N increases.

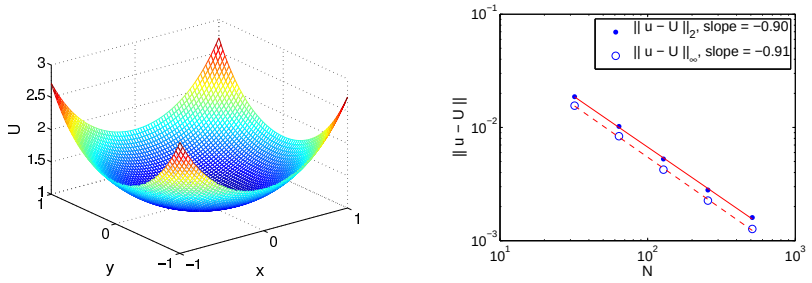

FIG. 6.2. *Example 2: Pure wide stencil. The exact solution is* $u(x,y) = e^{\frac{1}{2}(x^2+y^2)}$. *(1) Numerical solution. (2) Norms of the error* $\|u - \mathbf{U}\|$. *The convergence rates, indicated by the slopes, are close to* $O(h)$ *in both* L_2 *and* L_∞ *norms.*

N	$\|u-\mathbf{U}\|_2$	Numerical convergence rate	$\|u-\mathbf{U}\|_\infty$	Numerical convergence rate	Number of policy iterations
32	1.868×10^{-2}		1.557×10^{-2}		5
64	1.020×10^{-2}	0.87	8.364×10^{-3}	0.90	5
128	5.263×10^{-3}	0.95	4.240×10^{-3}	0.98	6
256	2.801×10^{-3}	0.91	2.259×10^{-3}	0.91	5
512	1.600×10^{-3}	0.81	1.268×10^{-3}	0.83	5

TABLE 6.2

Example 2: Pure wide stencil. The exact solution is $u(x,y) = e^{\frac{1}{2}(x^2+y^2)}$. *The convergence rates in both* L_2 *and* L_∞ *norms are close to* $O(h)$.

Example 2. Section 5 has proved that the local truncation error of the wide stencil discretization is $O(h)$ in the computational domain, and $O(\sqrt{h})$ near the boundary. In order to illustrate numerically the convergence rate of the wide stencil discretization, we still consider Example 1, but apply only the wide stencil discretization, instead of the mixed narrow/wide stencil discretization, on the entire computation domain. Figure 6.2 and Table 6.2 show that the convergence rate is close to first order, which is the optimal theoretical convergence rate for the pure wide stencil scheme. We note that the error using the mixed narrow/wide stencil scheme (Example 1) is significantly smaller than using the pure wide stencil scheme (Example 2), and the convergence rate using the mixed narrow/wide stencil scheme is faster.

Example 3. Consider

$$f(x,y) = \frac{1}{\sqrt{x^2+y^2}}, \qquad g(x,y) = \frac{2\sqrt{2}}{3}(x^2+y^2)^{\frac{3}{4}}, \qquad \Omega = [0,1]\times[0,1], \tag{6.5}$$

where f is singular at $(0,0)$, and the exact solution is

$$u(x,y) = \frac{2\sqrt{2}}{3}(x^2+y^2)^{\frac{3}{4}}. \tag{6.6}$$

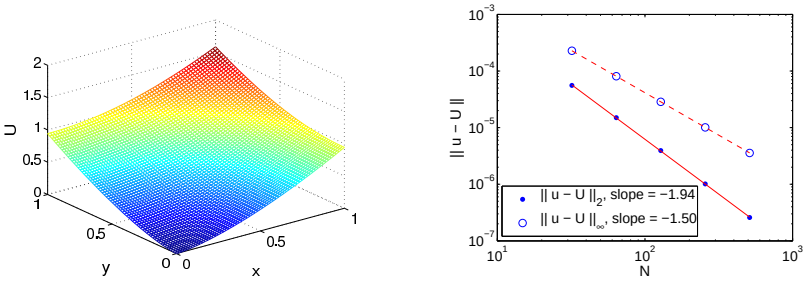

FIG. 6.3. *Example 3: Mixed narrow/wide stencil. The exact solution is* $u(x,y) = \frac{2\sqrt{2}}{3}(x^2+y^2)^{\frac{3}{4}}$. *(1) Numerical solution. (2) Norms of the error* $\|u-\mathbf{U}\|$. *The convergence rates, indicated by the slopes, are* $O(h^2)$ *in* L_2 *norm and* $O(h^{1.5})$ *in* L_∞ *norm, respectively.*

N	$\|u-\mathbf{U}\|_2$	Numerical convergence rate	$\|u-\mathbf{U}\|_\infty$	Numerical convergence rate	Number of policy iterations
32	5.561×10^{-5}		2.283×10^{-4}		4
64	1.498×10^{-5}	1.89	8.081×10^{-5}	1.50	4
128	3.930×10^{-6}	1.93	2.858×10^{-5}	1.50	4
256	1.014×10^{-6}	1.95	1.010×10^{-5}	1.50	4
512	2.588×10^{-7}	1.97	3.572×10^{-6}	1.50	4

TABLE 6.3

Example 3: Mixed narrow/wide stencil. The exact solution is $u(x,y) = \frac{2\sqrt{2}}{3}(x^2+y^2)^{\frac{3}{4}}$. *The convergence rates in* L_2 *and* L_∞ *norms are* $O(h^2)$ *and* $O(h^{1.5})$, *respectively.*

Similar to Example 1, since the optimal control pair (a^*,θ^*) at every grid point is inside $\Gamma^1\cup\Gamma^2\cup\partial\Gamma^0$, narrow stencil discretization can be applied monotonically on the entire Ω. The convergence rates in L_2 and L_∞ norm errors are $O(h^2)$ and $O(h^{1.5})$, respectively; see Figure 6.3 and Table 6.3.

Example 4. Consider

$$f(x,y) = \frac{2}{(2-x^2-y^2)^2}, \qquad g(x,y) = -\sqrt{2-x^2-y^2}, \qquad \Omega = [0,1]\times[0,1], \tag{6.7}$$

where f is singular at $(1,1)$, and the exact solution is

$$u(x,y) = -\sqrt{2-x^2-y^2}. \tag{6.8}$$

Once again, narrow stencil discretization can be applied monotonically on the entire Ω. The convergence rates are $O(h^2)$ and $O(h^{1.5})$ in L_2 and L_∞ norms respectively; see Figure 6.4 and Table 6.4.

Example 5. Consider

$$f(x,y) = \max\left(1-\frac{0.1}{\sqrt{x^2+y^2}},0\right), \qquad g(x,y) = \frac{1}{2}(\sqrt{x^2+y^2}-0.1)^2, \tag{6.9}$$
$$\Omega = [-0.5,0.5]\times[-0.5,0.5].$$

The exact solution is given by

$$u(x,y) = \frac{1}{2}\max\left(\sqrt{x^2+y^2}-0.1,0\right)^2. \tag{6.10}$$

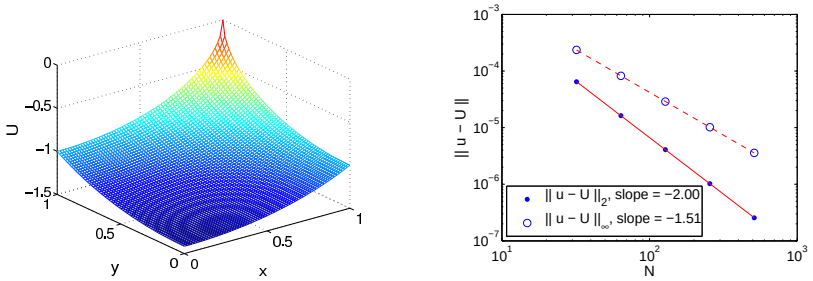

FIG. 6.4. *Example 4: Mixed narrow/wide stencil. The exact solution is* $u(x,y) = -\sqrt{2-x^2-y^2}$. *(1) Numerical solution. (2) Norms of the error* $\|u-\mathbf{U}\|$. *The convergence rates, indicated by the slopes, are* $O(h^2)$ *in* L_2 *norm and* $O(h^{1.5})$ *in* L_∞ *norm, respectively.*

N	$\|u-\mathbf{U}\|_2$	Numerical convergence rate	$\|u-\mathbf{U}\|_\infty$	Numerical convergence rate	Number of policy iterations
32	6.450×10^{-5}		2.359×10^{-4}		4
64	1.628×10^{-5}	1.99	8.211×10^{-5}	1.52	5
128	4.084×10^{-6}	2.00	2.882×10^{-5}	1.51	5
256	1.022×10^{-6}	2.00	1.015×10^{-5}	1.51	5
512	2.557×10^{-7}	2.00	3.583×10^{-6}	1.50	5

TABLE 6.4

Example 4: Mixed narrow/wide stencil. The exact solution is $u(x,y) = -\sqrt{2-x^2-y^2}$. *The convergence rates in* L_2 *and* L_∞ *norms are* $O(h^2)$ *and* $O(h^{1.5})$, *respectively.*

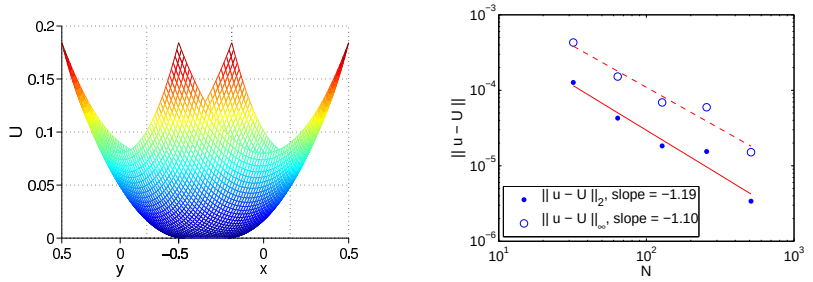

FIG. 6.5. *Example 5: Mixed narrow/wide stencil. The exact solution is* $\frac{1}{2}\max\left(\sqrt{x^2+y^2}-0.1,0\right)^2$. *(1) Numerical solution. (2) Norms of the error* $\|u-\mathbf{U}\|$. *The convergence rates, indicated by the slopes, are close to* $O(h)$ *in both* L_2 *and* L_∞ *norms.*

N	$\|u-\mathbf{U}\|_2$	Numerical convergence rate	$\|u-\mathbf{U}\|_\infty$	Numerical convergence rate	Number of policy iterations
32	1.270×10^{-4}		4.298×10^{-4}		4
64	4.273×10^{-5}	1.57	1.520×10^{-4}	1.50	6
128	1.835×10^{-5}	1.22	6.907×10^{-5}	1.14	7
256	1.544×10^{-5}	0.25	5.959×10^{-5}	0.21	9
512	3.396×10^{-6}	2.18	1.513×10^{-5}	1.98	20

TABLE 6.5

Example 5: Mixed narrow/wide stencil. The exact solution is $\frac{1}{2}\max\left(\sqrt{x^2+y^2}-0.1,0\right)^2$.

This is a C^1 function where the singularity occurs at the ring $x^2 + y^2 = 0.1^2$. Numerical results have been included in Figure 6.5 and Table 6.5. The error reduction rates for the sequence of $N = 32, 64, \cdots, 512$ do not look as regular as the previous examples. The explanation is that wide stencil has been applied near the ring $x^2 + y^2 = 0.1^2$. Wide stencil truncation error depends on both central differencing error and interpolation error, and usually interpolation error fluctuates as N increases, despite converging towards 0. However, a clear error reduction, and thus convergence, can be observed in Figure 6.5 and Table 6.5.

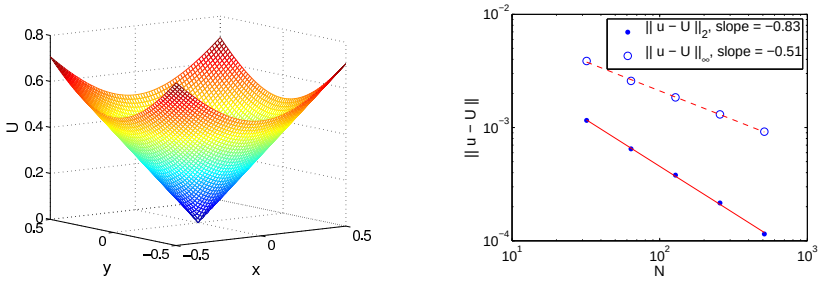

FIG. 6.6. *Example 6: Mixed narrow/wide stencil. The exact solution is* $u(x, y) = \sqrt{x^2 + y^2}$. *(1) Numerical solution. (2) Norms of the error* $\|u - \mathbf{U}\|$. *The convergence rates, indicated by the slopes, are* $O(h^{0.8})$ *in* L_2 *norm and* $O(h^{0.5})$ *in* L_∞ *norm, respectively.*

N	$\|u - \mathbf{U}\|_2$	Numerical convergence rate	$\|u - \mathbf{U}\|_\infty$	Numerical convergence rate	Number of policy iterations
32	1.156×10^{-3}		3.868×10^{-3}		9
64	6.484×10^{-4}	0.83	2.583×10^{-3}	0.58	15
128	3.803×10^{-4}	0.77	1.848×10^{-3}	0.48	17
256	2.159×10^{-4}	0.82	1.305×10^{-3}	0.50	23
512	1.148×10^{-4}	0.91	9.203×10^{-4}	0.50	27

TABLE 6.6

Example 6: Mixed narrow/wide stencil. The exact solution is $u(x, y) = \sqrt{x^2 + y^2}$. *The convergence rates in* L_2 *and* L_∞ *norms are* $O(h^{0.8})$ *and* $O(h^{0.5})$, *respectively.*

Example 6. In this example, the corresponding f is a delta function at the origin and is zero elsewhere:

$$f(x, y) = \pi\delta(0, 0), \quad g(x, y) = \sqrt{x^2 + y^2}, \quad \Omega = [-0.5, 0.5] \times [-0.5, 0.5]. \tag{6.11}$$

The exact solution

$$u(x, y) = \sqrt{x^2 + y^2} \tag{6.12}$$

is a C^0 function, and is singular at the origin. Figure 6.6 shows that the mixed narrow/wide stencil scheme converges to the cone-shaped exact solution, and Table 6.6 shows the orders of convergence are close to 0.8 and 0.5 in L_2 and L_∞ norms respectively.

Example 7. In the last example, we show explicitly that non-monotone numerical scheme may converge to a non-viscosity solution (which may be non-convex). Hence, it matters to design a monotone numerical scheme that converges to the viscosity

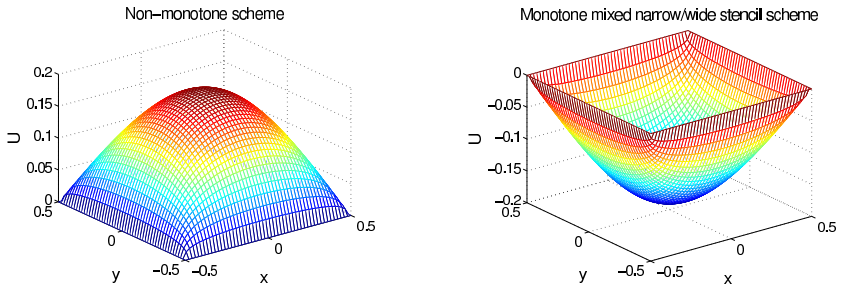

FIG. 6.7. *Example 7: (1) One possible solution given by a non-monotone scheme, which is concave and thus cannot be a viscosity solution. (2) The solution given by the monotone mixed narrow/wide stencil scheme, which is convex and is convergent in the viscosity sense.*

solution (which is convex). More analysis on this issue can be found in [14, 4]. We consider

$$f(x,y) = 1, \qquad g(x,y) = 0, \qquad \Omega = [-0.5, 0.5] \times [-0.5, 0.5], \tag{6.13}$$

where the exact solution is not available. This Dirichlet problem has a unique convex viscosity solution u^{visc}. It is easy to verify that the Dirichlet problem has more than one solution. For instance, the concave function $-u^{visc}$ is also a solution. Due to the uniqueness of the viscosity solution, any solution other than u^{visc} cannot be a viscosity solution.

A possible non-monotone discretization for $u_{xx}u_{yy} - u_{xy}^2 = f$ is the direct application of the standard central differencing:

$$\begin{aligned} &\left(\frac{U_{i+1,j} - 2U_{i,j} + U_{i-1,j}}{h^2}\right)\left(\frac{U_{i,j+1} - 2U_{i,j} + U_{i,j-1}}{h^2}\right) \\ &\quad - \left(\frac{U_{i+1,j+1} + U_{i-1,j-1} - U_{i+1,j-1} - U_{i-1,j+1}}{4h^2}\right)^2 = f_{i,j}. \end{aligned} \tag{6.14}$$

In our numerical experiment, we find out that the numerical solution under the non-monotone discretization converges to a concave function. We note that [4] has considered the same example using non-monotone discretization, and obtained another non-viscosity solution that is non-convex near the corner of Ω. Conversely, the numerical solution using our monotone narrow/wide stencil discretization converges to the convex viscosity solution (Figure 6.7).

Appendix A. Proof of Lemma 2.2.

To prove Lemma 2.2, we start with the simplest case - both A and B are diagonal matrix.

LEMMA A.1. *Let* $\tilde{B} = \begin{pmatrix} b_1 & \\ & b_2 \end{pmatrix}$ *be a* 2×2 *diagonal matrix, and let* $c \geq 0$. *Define the set*

$$T_1^+ \equiv \left\{ \tilde{A} = \begin{pmatrix} a_1 & \\ & a_2 \end{pmatrix}, \tilde{A} \text{ is positive semi-definite}, \operatorname{tr}(\tilde{A}) = 1 \right\}. \tag{A.1}$$

Then $\tilde{B}$ *satisfies*

$$\max_{\tilde{A}\in T_1^+} \left\{ \operatorname{tr}(\tilde{A}\tilde{B}) + c\sqrt{\det(\tilde{A})} \right\} = 0, \tag{A.2}$$

if and only if

$$\begin{aligned} &\tilde{B} \text{ is negative definite,} \\ &2\sqrt{\det(-\tilde{B})} = c. \end{aligned} \tag{A.3}$$

Proof. The proof of $c = 0$ is straightforward and we leave it to the readers. Here we focus on $c > 0$. T_1^+ can be simplified as:

$$T_1^+ = \left\{ \tilde{A} = \begin{pmatrix} a & \\ & 1-a \end{pmatrix},\ a \in [0,1] \right\}. \tag{A.4}$$

Define the objective function

$$\mathcal{O}(a) \equiv \mathrm{tr}(\tilde{A}\tilde{B}) + c\sqrt{\det(\tilde{A})} = ab_1 + (1-a)b_2 + c\sqrt{a(1-a)}. \tag{A.5}$$

The stationary point of $\mathcal{O}(a)$, denoted as a^*, is given by

$$\frac{\partial}{\partial a}\mathcal{O}(a^*) = 0 \quad \Rightarrow \quad a^* = \frac{1}{2}\left(1 + \frac{b_1 - b_2}{\sqrt{c^2 + (b_1 - b_2)^2}}\right). \tag{A.6}$$

Note that when $c > 0$, $a^* \in (0,1)$. Also the second derivative is

$$\frac{\partial^2}{\partial^2 a}\mathcal{O}(a) = -\frac{c}{4[a(1-a)]^{3/2}} < 0, \quad a \in (0,1), \tag{A.7}$$

showing that $\mathcal{O}(a)$ is strictly concave at $a \in (0,1)$. Hence, a^* is the global maximum at $a \in [0,1]$.

(i) We will prove that (A.3) $\Rightarrow$ (A.2). Equation (A.3) can be written as

$$b_1 < 0, \quad b_2 < 0, \quad 2\sqrt{b_1 b_2} = c. \tag{A.8}$$

Under these conditions, the global maximum a^* in (A.6) becomes

$$a^* = \frac{b_2}{b_1 + b_2}. \tag{A.9}$$

One can verify that this a^* satisfies $\mathcal{O}(a^*) = 0$, so

$$\max_{a \in [0,1]} \mathcal{O}(a) = 0, \tag{A.10}$$

which is (A.2).

(ii) We will also prove that (A.2) $\Rightarrow$ (A.3). Start with (A.2),

$$\max_{a \in [0,1]} \mathcal{O}(a) = 0, \qquad \Rightarrow \qquad \mathcal{O}(a) \le 0,\ \mathcal{O}(a^*) = 0, \tag{A.11}$$

where a^* is given by (A.6). Since when $c > 0$, $a^* \neq 0$ or 1. This gives $\mathcal{O}(1) = b_1 < 0$, $\mathcal{O}(0) = b_2 < 0$, indicating that B is negative definite.

Let $a_0 = \frac{b_1^{-1}}{b_1^{-1} + b_2^{-1}}$. Considering that $\mathcal{O}(a_0) \le 0$, we obtain

$$0 \ge \mathcal{O}(a_0) = \frac{2b_1 b_2}{b_1 + b_2} - c\frac{\sqrt{b_1 b_2}}{b_1 + b_2}, \tag{A.12}$$

which leads to one inequality

$$2\sqrt{b_1 b_2} \geq c. \tag{A.13}$$

Also, by applying the geometric-arithmetic mean inequality at the optimal point a^*,

$$\begin{aligned} 0 &= \mathcal{O}(a^*) \\ &= a^* b_1 + (1-a^*) b_2 + c\sqrt{a^*(1-a^*)} \\ &= -|a^* b_1 + (1-a^*) b_2| + c\sqrt{a^*(1-a^*)} \\ &\leq -2\sqrt{a^* b_1 (1-a^*) b_2} + c\sqrt{a^*(1-a^*)}, \end{aligned} \tag{A.14}$$

we obtain the other inequality

$$2\sqrt{b_1 b_2} \leq c. \tag{A.15}$$

The inequalities (A.13) and (A.15) yield

$$2\sqrt{b_1 b_2} = c \quad \Rightarrow \quad 2\sqrt{\det(-\tilde{B})} = c, \tag{A.16}$$

which is Equation (A.3). ∎

To move one step forward, we consider the case where $\tilde{B}$ is diagonal while the set of A is expanded to S_1^+.

LEMMA A.2. *Let* $\tilde{B} = \begin{pmatrix} b_1 & \\ & b_2 \end{pmatrix}$ *be a* 2×2 *diagonal matrix, and let* $c \geq 0$. $\tilde{B}$ *satisfies*

$$\max_{A \in S_1^+} \left\{ \operatorname{tr}(A\tilde{B}) + c\sqrt{\det(A)} \right\} = 0, \tag{A.17}$$

if and only if

$$\begin{aligned} &\tilde{B} \text{ is negative definite,} \\ &2\sqrt{\det(-\tilde{B})} = c. \end{aligned} \tag{A.18}$$

where S_1^+ *is defined in (2.4).*

Proof. Let $A' = \begin{pmatrix} a_{11} & \\ & a_{22} \end{pmatrix}$ be the diagonal part of the matrix $A = \begin{pmatrix} a_{11} & a_{12} \\ a_{21} & a_{22} \end{pmatrix}$. It is easy to verify that if $A \in S_1^+$, then $A' \in T_1^+ \subset S_1^+$.

Since $\tilde{B}$ is diagonal, $\operatorname{tr}(A\tilde{B}) = \operatorname{tr}(A'\tilde{B})$. Also, since $\det(A) \leq \det(A')$, we have

$$\operatorname{tr}(A\tilde{B}) + c\sqrt{\det(A)} \leq \operatorname{tr}(A'\tilde{B}) + c\sqrt{\det(A')}, \quad \forall A \in S_1^+. \tag{A.19}$$

This leads to the following:

$$\max_{A \in S_1^+} \left\{ \operatorname{tr}(A\tilde{B}) + c\sqrt{\det(A)} \right\} = \max_{A' \in S_1^+} \left\{ \operatorname{tr}(A'\tilde{B}) + c\sqrt{\det(A')} \right\}. \tag{A.20}$$

Finally, notice that both A' and $\tilde{B}$ are diagonal, we can complete the proof by Lemma A.1. ∎

Proof of Lemma 2.2. If $B \in \mathbb{R}^{2\times 2}$ is a symmetric matrix, there exists an orthogonal matrix $Q \in \mathbb{R}^{2\times 2}$, such that $B = Q\tilde{B}Q^T$ where $\tilde{B}$ is a diagonal matrix. Also, since $A \in S_1^+$, we have $A^Q = Q^T AQ \in S_1^+$. This follows

$$\max_{A\in S_1^+}\left\{\mathrm{tr}(AB) + c\sqrt{\det(A)}\right\} = \max_{A^Q\in S_1^+}\left\{\mathrm{tr}(A^Q\tilde{B}) + c\sqrt{\det(A^Q)}\right\}. \tag{A.21}$$

Now the problem is reduced to Lemma A.2, which completes the proof.

Lemma A.1, A.2 and 2.2 can all be generalized to any finite dimension d. We refer the interested readers to [17] and [25].

REFERENCES

[1] *Monge-Ampère equation: applications to geometry and optimization*, vol. 226 of Contemporary Mathematics, American Mathematical Society, Providence, RI, 1999. Edited by Luis A. Caffarelli and Mario Milman.

[2] P. Azimzadeh and P. A. Forsyth, *Weakly Chained Matrices, Policy Iteration, and Impulse Control*, SIAM J. Numer. Anal., 54 (2016), pp. 1341–1364.

[3] G. Barles and P. E. Souganidis, *Convergence of approximation schemes for fully nonlinear second order equations*, Asymptotic Anal., 4 (1991), pp. 271–283.

[4] Jean-David Benamou, Brittany D. Froese, and Adam M. Oberman, *Two numerical methods for the elliptic Monge-Ampère equation*, M2AN Math. Model. Numer. Anal., 44 (2010), pp. 737–758.

[5] Klaus Böhmer, *On finite element methods for fully nonlinear elliptic equations of second order*, SIAM J. Numer. Anal., 46 (2008), pp. 1212–1249.

[6] Olivier Bokanowski, Stefania Maroso, and Hasnaa Zidani, *Some convergence results for Howard's algorithm*, SIAM J. Numer. Anal., 47 (2009), pp. 3001–3026.

[7] Susanne C. Brenner, Thirupathi Gudi, Michael Neilan, and Li-yeng Sung, *C^0 penalty methods for the fully nonlinear Monge-Ampère equation*, Math. Comp., 80 (2011), pp. 1979–1995.

[8] Michael G. Crandall, Hitoshi Ishii, and Pierre-Louis Lions, *User's guide to viscosity solutions of second order partial differential equations*, Bull. Amer. Math. Soc. (N.S.), 27 (1992), pp. 1–67.

[9] Michael G. Crandall and Pierre-Louis Lions, *Viscosity solutions of Hamilton-Jacobi equations*, Trans. Amer. Math. Soc., 277 (1983), pp. 1–42.

[10] E. J. Dean and R. Glowinski, *Numerical methods for fully nonlinear elliptic equations of the Monge-Ampère type*, Comput. Methods Appl. Mech. Engrg., 195 (2006), pp. 1344–1386.

[11] Kristian Debrabant and Espen R. Jakobsen, *Semi-Lagrangian schemes for linear and fully non-linear diffusion equations*, Math. Comp., 82 (2013), pp. 1433–1462.

[12] Xiaobing Feng and Michael Neilan, *Vanishing moment method and moment solutions for fully nonlinear second order partial differential equations*, J. Sci. Comput., 38 (2009), pp. 74–98.

[13] Peter A Forsyth and George Labahn, *Numerical methods for controlled Hamilton-Jacobi-Bellman PDEs in finance*, Journal of Computational Finance, 11 (2007), p. 1.

[14] Brittany D. Froese and Adam M. Oberman, *Convergent finite difference solvers for viscosity solutions of the elliptic Monge-Ampère equation in dimensions two and higher*, SIAM J. Numer. Anal., 49 (2011), pp. 1692–1714.

[15] Cristian E Gutiérrez, *The Monge-Ampère Equation*, vol. 42, Springer Science & Business Media, 2012.

[16] Ronald A. Howard, *Dynamic programming and Markov processes*, The Technology Press of M.I.T., Cambridge, Mass.; John Wiley & Sons, Inc., New York-London, 1960.

[17] N. V. Krylov, *The control of the solution of a stochastic integral equation*, Teor. Verojatnost. i Primenen., 17 (1972), pp. 111–128.

[18] Randall J. LeVeque, *Finite difference methods for ordinary and partial differential equations*, Society for Industrial and Applied Mathematics (SIAM), Philadelphia, PA, 2007. Steady-state and time-dependent problems.

[19] P.-L. Lions, *Hamilton-Jacobi-Bellman equations and the optimal control of stochastic systems*, in Proceedings of the International Congress of Mathematicians, Vol. 1, 2 (Warsaw, 1983), PWN, Warsaw, 1984, pp. 1403–1417.

[20] K Ma and P Forsyth, *An unconditionally monotone numerical scheme for the two factor uncertain volatility model*, Preprint, (2014).

[21] Adam M. Oberman, *Wide stencil finite difference schemes for the elliptic Monge-Ampère equation and functions of the eigenvalues of the Hessian*, Discrete Contin. Dyn. Syst. Ser. B, 10 (2008), pp. 221–238.

[22] V. I. Oliker and L. D. Prussner, *On the numerical solution of the equation* $(\partial^2 z/\partial x^2)(\partial^2 z/\partial y^2) - ((\partial^2 z/\partial x \partial y))^2 = f$ *and its discretizations. I*, Numer. Math., 54 (1988), pp. 271–293.

[23] Yousef Saad, *Iterative methods for sparse linear systems*, Society for Industrial and Applied Mathematics, Philadelphia, PA, second ed., 2003.

[24] P. N. Shivakumar, Joseph J. Williams, Qiang Ye, and Corneliu A. Marinov, *On two-sided bounds related to weakly diagonally dominant M-matrices with application to digital circuit dynamics*, SIAM J. Matrix Anal. Appl., 17 (1996), pp. 298–312.

[25] Iain Smears, *Hamilton-Jacobi-Bellman equations analysis and numerical analysis*, tech. report, research report available on `www.math.dur.ac.uk/Ug/projects/highlights/PR4/Smears_HJB_report.pdf`.

[26] J. Wang and P. A. Forsyth, *Maximal use of central differencing for Hamilton-Jacobi-Bellman PDEs in finance*, SIAM J. Numer. Anal., 46 (2008), pp. 1580–1601.